Chapter 2
Mineralogy

Potassium-rich silica-undersaturated mafic igneous rocks are characterised by the presence of leucite, K-feldspar, clinopyroxene and Fe–Ti oxides. Plagioclase feldspar commonly appears in tephrites, tephritic phonolites, and phonolitic tephrites. In sodium-rich potassic rocks such as basanites, forsteritic olivine appears along with nepheline. Whereas in lamproites and lamprophyres, phlogopite is a very common mineral, K-richterite may also appear along with the above-mentioned minerals (Wagner and Velde 1986). In mildly sodium-rich potassic rocks, nepheline-kalsilite solid solutions are commonly observed. Kalsilite is particularly present in mafuritic rocks. Melilite, whenever present, is formed by reaction between clinopyroxene and nepheline (Bowen 1922; Schairer et al. 1962); haüyne and sodalites may be accompanying phases along with them analcite occurs as an alteration product of leucite. Pseudo-leucite (an intergrowth of nepheline and K-feldspar) may occur instead of leucite in rocks emplaced before the Tertiary period. Priderite and wadeite are two accessory phases commonly associated with lamproitic rocks. Mg-spinel ($MgAl_2O_4$), perovskite, titanomagnetite, pseudo-brookite, ilmenite, chromite, a roedderite-like mineral and apatite are other accessory phases. Recently, Mihajlovic et al. (2002) have reported the occurence of two accessory minerals rondorfite, $Ca_8Mg[SiO_4]_4Cl_2$, and almarudite, $K\square(Na)_2(Mn,Fe,Mg)_2(Be,Al)_3[Si_{12}O_{30}]$, and a iron-rich wadalite, $Ca_{12}[(Al_8Si_4Fe_2)O_{32}]Cl_6$, from the Bellerberg (Bellberg) volcano, Eifel, Germany. Carbonates (a solid solution of $CaCO_3$, $MgCO_3$ and $FeCO_3$) occur quite often as groundmass phases. Melanite garnets are also rarely observed.

2.1 Leucite

This mineral has a cubic symmetry at temperatures higher than 630 °C, but below this temperature, it becomes tetragonal. Most leucite grains therefore, show repeated twinning on the (110) crystallographic plane, which is related to cubic-tetragonal inversion. The heat capacity measurements indicate that the transition is continuous and of second order (Lange et al. 1986). Gatta et al. (2008) studied

A.K. Gupta, *Origin of Potassium-rich Silica-deficient Igneous Rocks*,
Springer Geology, DOI 10.1007/978-81-322-2083-1_2

elastic and structural behaviour of a natural tetragonal leucite from the volcanic Lazium district (Italy). Their investigation at high pressure by an in situ single-crystal X-ray diffraction with a diamond anvil cell under hydrostatic conditions, showed a first-order phase transition, never reported in the literature before. They observed the transformation from tetragonal to triclinic symmetry at $P = 2.4 \pm 0.2$ GPa. The phase transformation is accompanied by a drastic increase in density of about 4.7 %.

In slightly older rocks, leucite is often altered to pseudoleucite by reaction with a Na-rich fluid (Gupta and Fyfe 1975). Hovis et al. (2002) have studied two synthetic solid-solution series, namely, analcime to Rb-leucite and analcime to Cs-leucite (pollucite) to understand more fully the thermodynamic and structural behaviour of analcime-leucite and similar mineral systems. Unit-cell dimensions and volumes in these series expand with the substitution of analcime component in either Rb-leucite or pollucite, as H_2O molecules structurally replace Rb or Cs. Unit-cell volumes of the above two minerals vary linearly as a function of composition. During symmetry changes from tetragonal to isometric, as in the Rb-bearing series, the slope of the volume expansion curve changes. Once structures have reached full expansion, slopes related to volume changes flatten and are little affected by additional analcime component. Overall, the data suggest that the analcime-leucite system also can be modelled as close to thermodynamically ideal. The limited solid solution between natural analcime and leucite must be attributed to energetically favored heterogeneous equilibria involving minerals such as feldspars and other feldspathoids, and there is limited immiscibility between the end-members.

Leucite incorporates up to 28 wt% $NaAlSi_2O_6$ (Fig. 2.1) at 0.1 GPa [$P(H_2O) = P$ (Total)] and 800 °C in the join $KAlSi_2O_6$–$NaAlSi_2O_6$ (Fudali 1963). Natural leucite does not contain more than 10 wt% $NaAlSi_2O_6$. Leucites from Leucite Hills incorporate excess silica and alkali over alumina and ferric ion (Carmichael 1967; Barton 1979). It contains up to 8 wt% $KAlSi_3O_8$ at 0.1 GPa [$P(H_2O) = P$(Total)] and 800 °C (Fudali 1963), and less than 5 wt% $NaAlSi_3O_8$ at 1 atmosphere and 800 °C (Gupta and Yagi 1980). It was observed by the latter workers that up to 6 wt% of $KFe^{3+}Si_2O_6$ is incorporated at 1 atmosphere, but it increases to 7.7 wt% under 0.2 GPa in presence of excess water. Deer et al. (1963) reported up to 1 wt% CaO in leucite from the East African Rift valley. Schairer (1948) confirmed that extensive substitution of Mg occurs in the leucite structure, where the following type of substitution takes place: Mg, Si ≈ Al, Al.

Phenocrystal leucites in mafic phonolites from Highwood Mountains are rare, and often replaced by analcite. Pseudoleucites are also observed in the rocks from this locality. Pure leucite however, occurs inside salite crystals. Such leucites contain minor Fe, Ca, Ba and Na (0.05–0.4 wt%).

Kuehner et al. (1981) observed that a leucite from Leucite Hills (U.S.A.) contain up to 2.90 wt% Fe_2O_3. The leucites incorporate 1,549–2,990 ppm Ba, 306–439 ppm Zr, 309–418 ppm Sr and 436–555 ppm Rb. Leucite is rarely preserved in the Brown Tuffaceous Pumice (Roccamonfina; Luhr and Giannetti 1987), and analcitization of leucite is common in such rocks.

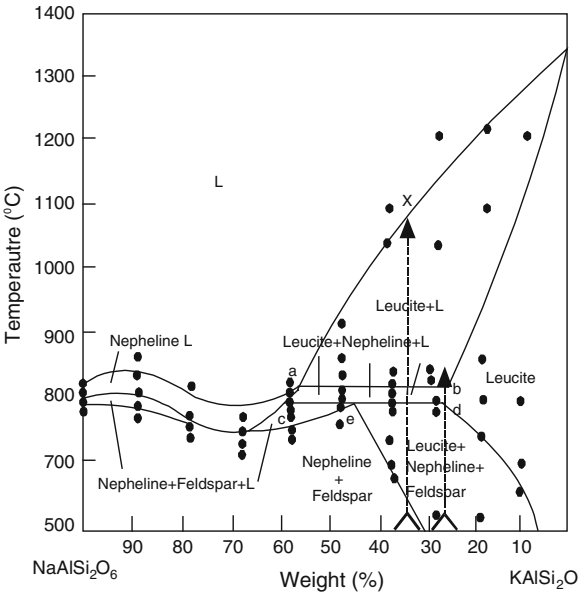

Fig. 2.1 Phase diagram of the system $KAlSi_2O_6$–$NaAlSi_2O_6$ under 0.1 GPa $P(H_2O)$ (after Fudali 1963)

The lavas of Alban Hills, central Italy, often contain fresh leucite crystals with near theoretical composition having 0.27 wt% Na_2O (Table 2.1, Francalanci et al. 1987). They are unzoned and do not have excess silica as observed in leucites from Vico and Vulsini (Holm et al. 1982).

The Gaussberg lavas have leucite crystals, which are generally twinned indicating a slow rate of cooling through the cubic-tetragonal inversion temperature. The compositional range is small and is very close to ideal leucite stoichiometry (Sheraton and Cundari 1980). They did not observe any significant difference in chemistry (Table 2.1). There is also significant amount of Ba (up to 0.3 wt% BaO) in the leucites of Gaussberg lamproites.

Vico lavas (Cundari 1975) have ubiquitous leucites, which show variable crystal development within and between flows from micro-crystalline to phenocrystal phase (1.5 cm across). Leucite often shows signs of resorption, and in rare cases is altered to analcite. Their K_2O content falls within the range of 17.6–20.0 wt%. The Na/K ratio varies significantly from 0.013 to 0.057 wt% even in leucites from the same rock specimen. A phenocrystal core has higher Na/K ratio than the rim. This observation is in agreement with the leucite data of Carmichael et al. (1974) from the similar lava type of the Roman region. The Vico leucites, however, show excess silica over the experimentally determined leucite solid solution (Fudali 1963). The extent of $NaAlSi_2O_6$ in Vico leucites varies from 1.1 to 5.0 wt% (Cundari 1975). Excess silica in leucite has also been reported by Brown and Carmichael (1969) from Korath Range and by Cundari (1973) from New South Wales.

Table 2.1 Analyses of leucite from different localities

	SiO_2	TiO_2	Al_2O_3	Fe_2O_3	FeO[a]	MgO	CaO	BaO	Na_2O	K_2O	Total
1	54.54	0.08	21.13		0.36				0.05	21.33	97.49
2	55.42	0.04	23.71		0.51				0.027	21.27	101.15
3	54.16	0.05	21.85		0.76				0.11	22.59	99.27
4	55.90	0.08	20.70		1.27	0.18	0.05	0.01	0.33	21.20	99.72
5	56.00	0.14	21.50		0.58	0.06	0.03	0.01	0.22	21.20	99.74
6	54.00	0.13	22.30		0.63	0.08	0.09		0.42	21.60	99.25
7	54.47		23.42		0.40		0.01		0.12	21.12	99.54
8	54.18		23.64		0.44		0.03		0.20	20.25	99.78
9	57.96		18.38	2.90				0.04	0.04	21.13	100.45
10	59.54		18.27	2.67					0.18	19.60	100.26
11	57.71		19.62	2.03				0.09	0.05	20.77	100.27
12	58.60		18.70	2.20			0.04		0.06	20.70	100.30
13	56.30		20.30	2.00			0.03		0.03	21.50	100.20
14	55.00	0.23	23.70	0.45					0.07	20.70	100.15
15	54.70	0.17	24.20	0.52					0.21	20.14	99.94
16	55.50	0.16	22.20	0.95					0.13	21.04	99.98

(continued)

Table 2.1 (continued)

	SiO_2	TiO_2	Al_2O_3	Fe_2O_3	FeO[a]	MgO	CaO	BaO	Na_2O	K_2O	Total
17	55.30		23.00	0.63			0.03		0.39	20.90	100.20
18	55.00		23.20	0.37			0.04		0.62	20.70	100.00
19	55.00	0.21	21.40	0.96		0.28		0.09	0.10	21.80	99.84
20	54.20–55.60	0.13–0.32	20.40–22.60	0.85–1.30		0.18–0.41		0.27	0.21	20.30–22.70	

[a] FeO indicates total FeO + Fe_2O_3 contents

1–3 Leucites from Leucitites, Alban Hills, Italy (Francalanci et al. 1987)
4–6 Leucites from K-rich rocks of Sierra Nevada, van Kooten (1980)
7–8 Leucites from basanites, Laacher See Area, Germany (Duda and Schminke 1978)
9 Rim of a leucite from wyomingite, Leucite Hills, Wyoming, U.S.A. (Kuehner et al. 1981)
10 Leucite from an olivine orendite, South Table Mountain, Leucite Hills, Wyoming, U.S.A. (Kuehner et al. 1981)
11 Leucite from an orendite, North Table Mountain, Leucite Hills, Wyoming, U.S.A. (Kuehner et al. 1981)
12–13 Leucites from lamproitic rocks, Leucite Hills, Wyoming, U.S.A. (Carmicheal 1967)
14–15 Leucites from leucitites, Begargo Hills, New South Wales, Australia (Cundari 1973)
16–18 Leucites from basanites, Vesuvius (Baldridge et al. 1981)
19–20 Leucites from leucitites, Gaussberg, Antarctica (Sheraton and Cundari 1980)

The Miocene lamproites from the Fitzroy area, West Kimberley (Australia) have leucite phenocrysts, which are typically euhedral and are unaltered (Jaques and Foley 1985). They are weakly birefringent, twinned, and commonly contain inclusions of glass arranged in concentric zone. Most glassy rocks are strongly resorbed and embayed. Leucite phenocrysts containing aluminous spinel inclusions are amoeboid-shaped with strongly rounded coalesced aggregates.

Divalent cations replacing K in leucite is rare (Jaques and Foley 1985), but the CaO content in excess of 1 wt%, has been described from the K-rich volcanic rocks of the East African Rift Valley.

2.2 K-Feldspar

Sanidine is found in tephritic phonolites, phonolitic tephrites, trachytes and/or phonolites from different localities of Italy, Manchuria, Tristan da Cunha and Udsuryo Island. It is also reported from leucite-bearing minettes and lamproites as an essential mineral. For example, they occur in lamproitic rocks from Navajo, Highwood Mountains, Smoky Butte (all from U.S.A.), Spain and Damodar Valley (India). K-feldspar also occurs as minor constituents in K-rich rocks of New South Wales (Australia) and Birunga (equatorial Africa). Inclusion-free phenocrystal sanidine (up to 2.5 mm long) occurs in Brown Leucitic Tuffs from Roccamonfina (Luhr and Giannetti 1987).

K-feldspar and plagioclase coexist in leucite-bearing tephritic rocks of the Eifel region, Germany (Worner and Schminke 1984). Individual sanidine crystals in these rocks are homogeneous containing 75–90 mol% orthoclase (Table 2.2). The tie lines between plagioclase and K-feldspar (Fig. 2.2) suggest equilibrium between two types of feldspars. In this figure, composition of two types of feldspars (open and solid circles with tie lines) as determined by Worner and Schminke (1984) from Laacher See phonolites, is shown. Leucite-bearing minettes from Bearpaw Mountains, U.S.A., contain invariably sanidine ($Or_{43}Ab_{41}An_{16}$ to $Or_{93}Ab_5An_2$, Table 2.2, Macdonald et al. 1992). There is a tendency for the orthoclase content to increase with decreasing magnesia concentration in the bulk rock. These sanidines are Ba-rich containing 7 mol% celsian (Cn) molecule. The sanidines ($Or_{47}Ab_{42}An_6Cn_5$ to $Or_2An_{56}Ab_{41}Cn_1$) in Bearpaw latites have variable chemistry.

The Potassic rocks of Highwood Mountains comprise sanidines, which are by far the dominant feldspars in these rocks (O'Brien et al. 1991). They occur as euhedral phenocrysts in mafic phonolites and trachytes and in coarse-grained shonkinites and malignites. It ranges in composition from K-rich variety ($Or_{88}Ab_9Cn_2Sl_1$) to albitic sanidine ($Or_{64}Ab_{34}An_2$). Sometimes, hyalophane with up to 11.1 wt% BaO ($Or_{44}Ab_{29}Cn_{22}An_3Sl_2$), are present (Sl represents slawsonite, Sr-feldpar). In Highwood Baldy stock, perthitic and antiperthic intergrowths in feldspars ranging in composition from $Or_{88}Ab_{12}$to Ab_{100} are observed.

Table 2.2 Analyses of K-feldspar from K-rich localities

	SiO_2	TiO_2	Al_2O_3	Fe_2O_3	FeO[a]	CaO	Na_2O	K_2O	SrO	MgO	BaO	Total	An	Ab	Or	Cn	Sr-f
1	63.61		19.68		0.21	0.38	1.27	14.26	0.57		0.31	100.29	0.019	0.117	0.864		
2	63.98		19.45		0.13	0.35	2.26	13.41	0.04			99.62	0.017	0.20	0.783		
3	65.10		19.40		0.21	0.39	2.05	12.20			0.06	99.41	2.10	20.00	77.90		
4	64.80		19.00		0.19	0.53	2.14	13.40			0.12	100.18	2.60	19.00	78.40		
5	65.20		19.20		0.20	0.45	1.22	14.10			0.03	100.40	2.30	11.40	86.30		
6	64.30		19.20		0.71	1.06	1.96	12.80			0.08	100.11	5.40	17.90	76.70		
7	57.93		22.21		0.71	1.36	4.93	4.99	3.23		4.57	99.93	6.90	45.40	30.30	8.50	8.90
8	55.51		23.48		0.71	2.20	4.98	3.38	4.16		5.31	99.73	11.30	46.40	20.70	10.00	11.60
9	62.61	0.27	18.83	0.79		0.02	0.31	15.53		0.42	0.41	99.07					
10	64.23	0.41	15.16	2.48			0.66	14.88		0.54	1.92	99.42					
11	64.41	0.40	15.79	2.14			0.64	15.11		0.30	1.52	100.32					
12	63.40	0.09	16.70		1.42	0.20	2.71	13.50		0.03	0.29	98.14					
13	63.30	0.26	17.80		1.96	0.04	3.34	11.60		0.04	1.03	99.37					
14	64.80	0.12	19.20		0.35	0.83	6.74	7.56		0.83	0.05	99.67					
14	63.90	0.27	17.46	1.12			0.44	16.15		0.02	0.25	99.61					
16	63.11	0.22	14.49	3.17			0.32	16.20		0.20	0.08	97.79					

(continued)

Table 2.2 (continued)

	SiO_2	TiO_2	Al_2O_3	Fe_2O_3	FeO[a]	CaO	Na_2O	K_2O	SrO	MgO	BaO	Total	An	Ab	Or	Cn	Sr-f
17	63.61	0.33	15.76	1.93			0.55	15.83			1.21	99.22					
18	63.23	0.29	15.86	2.91			0.32	15.84		0.08	0.50	99.03					
19	64.63	0.07	18.24	0.20			0.56	15.97			0.34	100.01					

[a] Whenever FeO values are given, they indicate total FeO + Fe_2O_3 contents

1–3 K-feldspars from Leucitic Tuffs Roccamonfina, Italy (Luhr and Giannetti 1987)
3–6 K-feldspars from leucite tuffs, Latera Caldera, Italy (Turbeville 1993)
7–8 K-feldspars from Mt. Vulture complex, Italy (Melluso et al. 1996)
9–11 Sanidines from lamproites, Smoky Butte, Montana (Mitchell et al. 1987)
12–14 Sanidines from K-rich rocks of Sierra Nevada (van Kooten 1980)
15 K-feldspar from a Cancarix lamproite, Albacete, Spain (Wagner and Valde 1986)
16 K-feldspar from a Jumilla lamproite, Murcia, Spain (Wagner and Valde 1986)
17 K-feldspar from a Smoky Butte lamproite, Montana, U.S.A. (Wagner and Valde 1986)
18 K-feldspar from a Moon Canyon lamproite, Utah, U.S.A (Wagner and Valde 1986)
19 K-Feldspar from Sisco Lamproite, France (Wagner and Valde 1986)

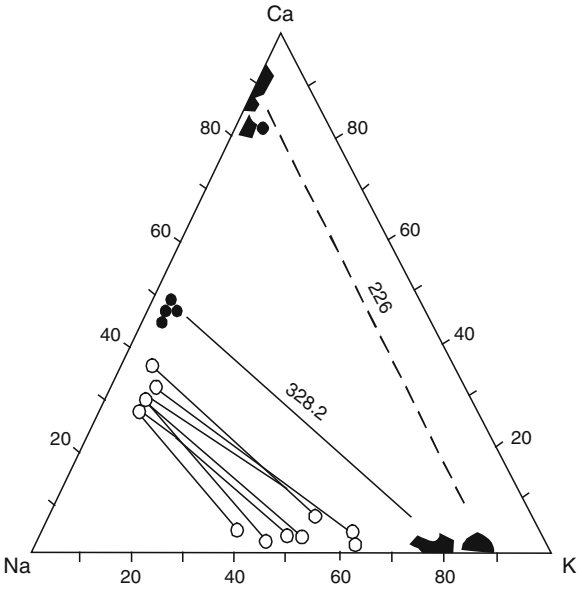

Fig. 2.2 Coexistence of calcic plagioclase in equilibrium with sanidine. There are two sets of alkali and plagioclase feldspars as shown by *solid* and *open circles*. The tie lines joining them suggest that two different types of feldspars are in equilibrium (after Worner and Schminke 1984)

The leucite-bearing rocks of Central Italy (Francalanci et al. 1987) have sanidines with compositions ranging between $Or_{88}Ab_{12}$ and $Or_{77}Ab_{23}$. The single crystals however, do not show compositional zoning. Such elements as Ba and Sr along with other trace elements, are present in appreciable amounts in K-feldspars. Perini et al. (2003) reported the presence of K-feldspar mega crysts hosted in K-rich rocks at Monte Ciminio volcanic complex Central Italy. These megacrysts are found in leucite-free olivine latites.

The highly potassic lavas from Latera Caldera (Roccamonfina, Italy) has sanidinse phenocrysts with compositions (Table 2.2) ranging from Or_{68} to Or_{90}. More potassic and Ba-rich variants are found in the phonolitic pumices. In Trachytic and phonolitic lavas, sanidine phenocrysts range in composition from $Or_{68}Ab_{32}$ to $Or_{90}Ab_{10}$. Sanidine crystals are observed also in trachytic pumices of Latera Caldera (Turbeville 1993). They are euhedral, unzoned and untwinned, containing <0.13 wt% BaO, and they are free from any mineral and glass inclusions. In tuffs of Latera Caldera sanidine phenocrysts ($Or_{69–82}$), are strongly embayed and include feldspar blebs with a compositional range of $Or_{63}Ab_{37}$–$Or_{74}Ab_{26}$. Chemical composition of sanidines from K-rich lavas of Vico, are in equilibrium with plagioclase. Wyoming Orendites and jumillte from Spain contain clear crystals of sanidine of variable sizes. These feldspars include diopside, leucite and rare apatite. The sanidine crystals from Leucite Hills, contain up to 18 % $KFeSi_3O_8$ molecule with very low amount of anorthite in solid solution (0.01–0.11 wt% CaO).

Lamproites from Mount North (Australia) are constituted of 19–48 vol% of K-feldspars containing 95–98 % Or. Those from Shiprock (Montana) contain 64–72 % orthoclase molecule, whereas those from Barqueros lamproites, Spain,

contain 87–89 % orthoclase (Wagner and Velde 1986). The average Fe_2O_3 content of K-feldspars is 1–2 %, but it is slightly higher in the Moon Canyon lamproite (2.5 %). Its concentration is as high as 0.62 % in Murcia lampoite and 1–3 % in Smoky Butte lamproite. In K-rich selagites from Orciatico (Italy) and Shiprock dyke (Montana), the BaO content shows large variation, 0–0.89 % and 0.3–3.32 %, respectively.

Coexistence of sanidine with anorthoclase, pseudoleucite and leucite is noted in shoshonitic and absarokitic rocks of Artem of Primorye district (north of Vladivostok), Russia. Here, K-feldspar constitutes 60–80 % of a potassic suite comprising nepheline, biotite, augite and amphibole (Borodin 1974). In many pseudoluecite tinguaites, syenites, and minette dykes at Pamir, K-feldspar occurs as a major phase (Dimitriev 1976). Sanidine is one of the major phases in the alkaline complex of the Tezhser in Caucasus, where it occurs in leucite-bearing trachytes and trachyandesites, where K-feldspar contains up to 10 % albite. Phase relations in the system kalsilite–K-feldspar at 2 GPa and variable temperatures are shown in Fig. 2.3, indicating limited solid solution of kalsilite in K-feldspar. Extent of solid solution of jadeite in K-feldspar (albite—K-feldspar) and jadeite in nepheline (nephiline—albite system) at 2 GPa and different temperatures are shown in Figs. 2.4 and 2.5, respectively.

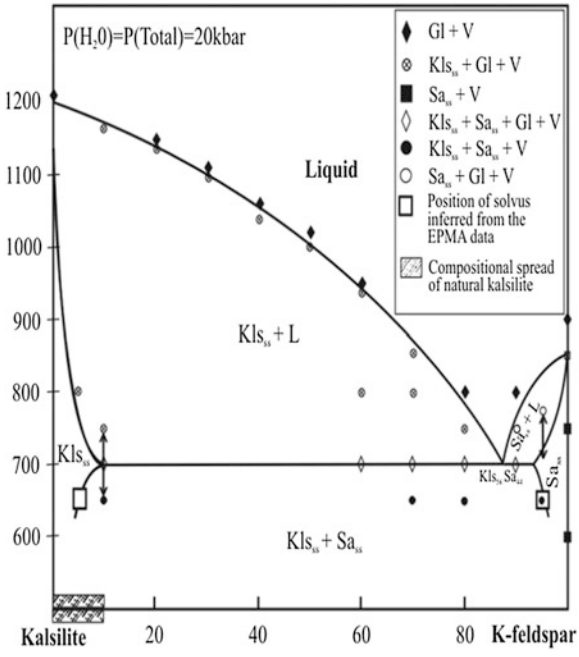

Fig. 2.3 Phase relations along the join kalsilite—K-feldspar determined at 2 GPa [$P(H_2O)$ = P(Total)] and various temperatures. The *solvus* has been inferred from EPMA data for *subsolidus* runs (after Gupta et al. 2010)

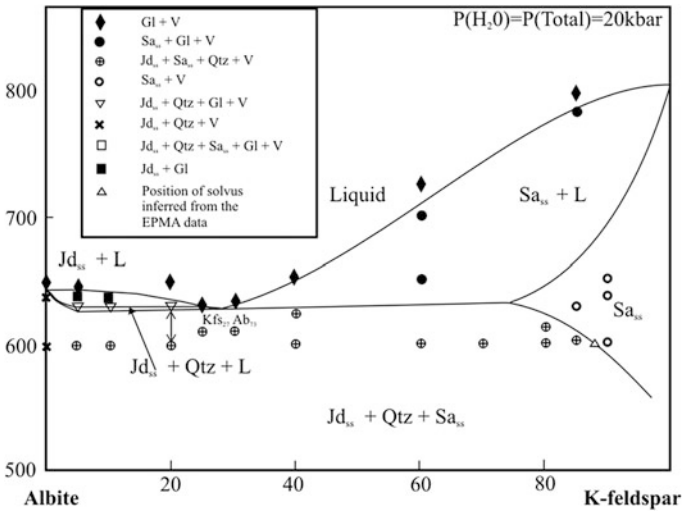

Fig. 2.4 Phase relations along the join albite—K-feldspar determined at 2 GPa [$P(H_2O)$ = P (Total)] and various temperatures (after Gupta et al. 2010)

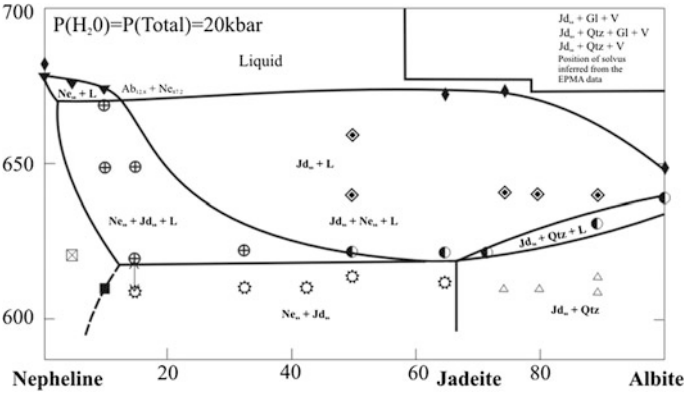

Fig. 2.5 Phase relations along the join nepheline–albite determined at 2 GPa [$P(H_2O)$ = P(Total)] and various temperatures (after Gupta et al. 2010)

2.3 Plagioclase

Plagioclase is a common mineral in leucite-bearing tephrites, basanites, tephritic phonolites and phonolitic tephrites of Vulsini, Vico, Sabatini and Somma-Vesuvius volcanic complexes, but it is absent in all lamproitic rocks. It is also found in the leucite-bearing rocks of Manchuria (China), Utsuryo islands (Korea) and Tristan da Cunha Islands. Plagioclase coexisting in equilibrium with leucite is calcium-rich

(Gupta and Edgar 1975). In their study of the join leucite-albite-anorthite under atmospheric pressure Gupta and Edgar showed that leucite does not coexist with pure albite, and reacts with it to produce nepheline$_{ss}$ and K–Na feldspar [(K, Na) $AlSi_3O_8$]. Nepheline, thus appears in the albite-rich portion of the join along with additional (K, Na) $AlSi_3O_8$.

Anorthite-rich plagioclase (up to 3 mm across) has been described from Brown Leucitic Tuffs of Roccamonfina by Luhr and Giannetti (1987). Most of the plagioclase crystals have compositions, plotting in the range of $An_{85–95}$ with a strong mode at $An_{87–89}$ (Fig. 2.2, Table 2.3). These plagiocases have up to 1 wt% SrO.

Mt. Vulture tephrites and phonolitic tephrites contain plagioclase, which occurs as a euhedral phase and is often enclosed within green salites together with leucite, haüyne and oxide minerals. In these rocks, the composition of plagioclase ranges (Table 2.3) continuously from An-rich (up to 81 vol%) through more sodic varieties to anorthoclase (Melluso et al. 1996). Plagioclase is found as microlites in basanites, tephrites and phonolitic tephrites. These plagioclase crystals are enriched in Sr and Ba (up to 4 wt% SrO and 7 wt% BaO). The Toppo S. Paolo phonolites are characterised by high concentration of Ba (7 wt% BaO and 2 wt% SrO). The plagioclase feldspars ($Or_5Ab_{55}An_{40}$) in minettes from Bearpaw Mountains are found to be in equilibrium with sanidine. The associated latites from the same locality contain plagioclase phenocrysts, which are idiomorphic and zoned ($Or_4Ab_{67}An_{29}$–$Or_5Ab_{68}An_{27}$).

The Latera Caldera of Roccamonfina (Italy) is known for eruption of phonolitic and tephri-phonolitic tuffs, which are constituted mainly of plagioclase crystals ($An_{77–87}$). These plagioclases are in general unzoned and unembayed in the wide pumices, whereas some of the black pumice fragments of overlying units have anorthitic plagioclases ($An_{72–93}$), which exhibit concentric zoning and more pronounced embayment and contain numerous minerals and glass inclusions. Plagioclase in Vico lavas (Cundari 1975) is occasionally glommeroporphyritic and strongly zoned and seldom resorbed (also Perini and Conticelli 2002). It is often a microphenocrystal phase. The plagioclase has anorthite content varying between 76.3 and 88.9 % in trachytic as well as tephritic phonolites.

In phonolitic tephrite of Ringgit Beser Complex of East Java (Edwards et al. 1991), the plagioclase feldspar coexisting in equilibrium with leucite, clinopyroxene and phlogopite are anorthite-rich (An_{91}).

2.4 Clinopyroxene

Diopside is the major component having variable amounts of $CaFeSi_2O_6$, $CaAl_2SiO_6$, $CaFe^{3+}AlSiO_6$, $NaCrSi_2O_6$ and $NaFeSi_2O_6$ molecules in solid solution. Orthopyroxene may be present in peridotite or pyroxenite xenoliths, but not in the silica-undersaturated potassic igneous rocks (for explanation, see Chap. 9).

Table 2.3 Analyses of plagioclase from different leucite-bearing localities

	SiO_2	Al_2O_3	FeO_t^a	BaO	SrO	MnO	CaO	Na_2O	K_2O	Total	An	Ab	Srf
1	45.47	34.39	0.69		0.76		17.41	1.60	0.29	100.61			
2	55.34	28.30	0.34		0.08		9.80	5.62	0.80	100.28			
3	55.40	28.60	0.55				9.95	5.21	0.87	100.58			
4	47.70	33.00	0.69		0.09		16.80	1.75	0.47	99.50			
5	53.50	28.40	0.60				12.30	4.10	0.83	99.73			
6	45.80	34.00	0.74			0.06	18.40	1.23	0.11	100.34			
7	46.10	33.00	0.75				18.30	1.63	0.14	99.92			
8	46.68	33.53	0.54		1.04		16.21	1.76	0.13	99.89	80.60	15.80	2.80
9	48.58	32.18	0.68		0.90		14.85	2.51	0.15	99.85	74.00	22.60	2.40

[a] FeO_t represents total FeO + Fe_2O_3 contents

1–2 Plagioclases from leucite tuffs, Roccamonfina (Luhr and Giannetti 1987)

3–5 Plagioclases from leucite tuffs, Latera Caldera (Turbeville 1993)

6–7 Pl agioclases from leucite tephrites Vico lavas (Cundari 1975)

8–9 Plagioclases from Mt. Vulture volcanic complex, Italy (Melluso et al. 1996)

Table 2.4 Analyses of clinopyroxenes From K-rich rocks of different localities

		SiO_2	TiO_2	Al_2O_3	Cr_2O_3	FeO_t^a	MnO	MgO	CaO	NiO	Na_2O	K_2O	Total
1	Core	50.32	0.77	3.81	0.28	6.27	0.08	14.16	24.43		0.16		100.16
2	Mantle	49.38	0.73	4.64	0.08	7.79		13.31	24.53		0.14		100.60
3	Rim	45.36	1.82	8.20	0.10	9.84	0.12	10.82	24.18		0.24		100.68
4	Core	44.87	1.66	8.61		9.16	0.14	10.80	24.24		0.66		100.14
5	Mantle	48.12	0.62	5.53	0.04	6.86	0.30	12.71	24.60		0.48		99.42
6	Rim	50.44	0.62	3.36	0.13	5.40	0.03	14.27	25.07		0.14		99.46
7	Core	43.80	1.52	10.3		11.00		10.00	23.80		0.33		100.75
8	Rim	45.20	1.28	8.90		9.65		11.30	23.40		0.45		100.18
9	Core	39.20	1.97	12.60		14.60	0.37	7.11	23.10		0.33		99.28
10	Mantle	45.50	1.52	8.71		10.80	0.27	9.67	23.40		0.53		100.40
11	Rim	43.30	1.51	7.59		16.30	0.87	6.93	22.70		0.80		100.00
12	Core	52.51	0.33	1.57		3.04	0.06	17.45	24.15		0.13		99.24
13	Mantle	47.83	1.02	5.67		10.49	0.33	11.26	23.70		0.47		100.77
14	Rim	46.73	1.04	6.33		10.87	0.28	11.15	23.82		0.44		100.66
15	Core	47.80	0.84	4.75		10.90	0.77	10.70	23.60		0.53		99.89
16	Mantle	43.00	2.00	9.62		10.80	0.09	10.50	23.30		0.23		99.54
17	Rim	46.10	1.36	5.57		10.80	0.54	10.20	24.90		0.44		99.91
18		54.55	0.79	0.38	0.01	2.31	0.14	16.61	25.45		0.16	0.09	100.49
19		54.20	0.51	0.05		2.08		17.92	24.96		0.20	0.01	99.93
20		51.84	0.19	1.59	0.03	10.89	0.42	12.05	22.50		0.47	0.02	100.00

(continued)

Table 2.4 (continued)

		SiO_2	TiO_2	Al_2O_3	Cr_2O_3	FeO_t^a	MnO	MgO	CaO	NiO	Na_2O	K_2O	Total
21	Core	54.28	1.69	0.22	0.38	3.18		17.83	22.10				99.68
22	Rim	54.01	2.18	0.25		3.92		17.53	22.10				99.99
23		53.00	0.92	0.52	0.56	4.30	0.12	16.70	23.30	0.06	0.39		99.87
24	Core	54.48	0.39	0.51		2.98	0.08	18.68	23.26				100.38
25	Rim	53.75	0.58	0.70		2.83	0.06	17.64	22.98				98.54
26		52.60	1.29	2.60		6.46	0.38	15.30	21.20	0.06	0.65	0.12	100.66

[a] FeO_t indicates total FeO + Fe_2O_3 content. Analyses of 18, 19, 20 and 26 are those of certain grains

1–3 Pyroxene phenocrysts (No. 1) (analyses of core, mantle and rim) from a tephritic rock of Alban Hills (Aurisicchio et al. 1988)

4–6 Pyroxene phenocrysts (No. 2) (analyses of core, mantle and rim) from a tephritic rock of Alban Hills (Aurisicchio et al. 1988)

7–8 Pyroxene phenocrysts (No. 1) (analyses of core, mantle and rim) from a leucite tephrite, Vulsini, Italy (Barton et al. 1982)

9–11 Pyroxene phenocrysts (No 2) (analyses of core, mantle and rim) from a leucite tephrite, Vulsini, Italy (Barton et al. 1982)

12–14 Clinopyrexenes from Brown Leucitic Tuffs, Roccamonfina (Luhr and Giannetti 1987)

15–17 Clinopyroxenes from a phonolitic pumice clast, Latera Caldera, Italy (Turbeville 1993)

18 Core of a pyroxene phenocryst from an orendite obtained from North Table Mountain, Leucite Hills (Kuehner et al. 1981)

19 A pyroxene grain from a wyomingite obtained from Zirkel Mesa, Leucite Hills (Kuehner et al. 1981)

20 A pyroxene grain from a wyomingite obtained from Spring Butte, Leucite Hills (Kuehner et al. 1981)

21–22 Clinopyroxenes from a lamproite, Smoky Butte, U.S.A. (Mitchell et al. 1987)

23 A clinopyroxene grain from a leucitite, Gaussberg, Greenland (Sheraton and Cundari 1980)

24–25 Diopsidic pyorxenes form an ultrapotassic rock of Spain (Lopez Ruiz, Badiola 1980)

26 Clinopyroxene from an ultrapotassic rock of Sierra Nevada (van Kooten 1980)

The lamproites from southern Spain, Smoky Butte (Montana, U.S.A.), Shiprock dyke (New Mexico, U.S.A.), Moon Canyon (Utah, U.S.A.), Sisco (Corsica), Mount North (West Kimberley, Australia) and Orciatico (Pisa, Italy) mostly plot in the endiopside field of the pyroxene quadrilateral (Wagner and Velde 1986). This mineral constitutes 6–22 wt% in a lamproite. The pyroxenes in lamproites, often occur as unzoned phenocrysts containing around 1 wt% TiO_2 and 0.1–0.3 wt% Cr_2O_3.

With the exception of Shiprock lamproite (Smoky Butte), the tetrahedral site of the pyroxenes is incompletely filled by Si and Al, average being 1.97–1.93 atom (Wagner and Velde 1986). The vacancy may be filled by remaining Fe^{3+}, when structural formula is calculated in terms of four cations and six oxygens. This deficiency in the tetrahedral site was also noticed in lamproites of Leucite Hills, Wyoming, U.S.A. (Carmichael 1967) and West Kimberley, Australia (Jaques et al. 1984). Acmite is present in many samples as a thin rim around diopside crystals. Wagner and Velde noted the presence of a green centre (enriched in Al, Fe and Na) in diopside phenocrysts of Shiprock lamproites. Similar green centre in pyroxenes of salite composition, has been described from Leucite Hills by Barton and van Bergen (1981). Such green-centred pyroxenes are considered to be disaggregation products of clinopyroxene nodules, and are common features in potassic volanics.

The K-rich lamproites of North Table Mountain at Zirkel Mesa and Spring Boat (both from Leucite Hills, Wyoming, U.S.A., Kuehner et al. 1981) contain predominantly diopside, but those from some wyomingites have salite cores, rimmed by diopsides (Table 2.4).

The clinopyroxenes from the minette dykes of Highwood Mountains are mainly diopsides ($Wo_{46}En_{46}Fs_8$) containing up to 2 wt% Cr_2O_3 (O'Brien et al. 1991), but they also occur in the salite cores of minettes from this area. Salites ($Wo_{47}En_{40}Fs_{13}$) from mafic phonolites and syenites of Highwood Mountains grade to ferrosalite and acmite. The Ti, Al and Na contents in pyroxenes increase with decreasing Cr contents. All pyroxenes have Fe^{3+}/Fe^{2+} ratios >1. The mantle and halos of salites (surrounding cavities in diopside cores) contain abundant inclusions of biotite, leucite, titanomagnetite and apatite, and all pyroxenes have a fassaitic rim, grown along different sector zones. Oscillatory zoning and diffusion halos in salites are common in potassic rocks of the Highwood Mountains region. Such halos are found as patches in Mg-rich salites. In both types of salites, the reacted margins are more Mg-rich than the [001] sectors of the unrelated crystals. This type of dissolution is commonly restricted to a single zone sector (001). In some cases the partially dissolved crystals are overgrown by more Fe-rich salite rims (O'Brien et al. 1991).

The K-rich rocks of the Alto Paranaiba Igneous Province are characterised mainly by diopsidic pyroxenes ($Ca_{48}Mg_{46}Fe_6$) containing minor amount of enstatite or hedenbergite in solid solution. The low Al and variable Ti contents of clinopyroxenes from Alto Paranaiba are similar to those of clinopyroxenes from lamproites of West Kimberley (Australia) and Kapamba (Zambia). Clinopyroxenes from Brown Leucitic Tuffs of Roccamonfina (Luhr and Giannetti 1987) are green unzoned salites, which are quite homogeneous in composition. In addition to salite,

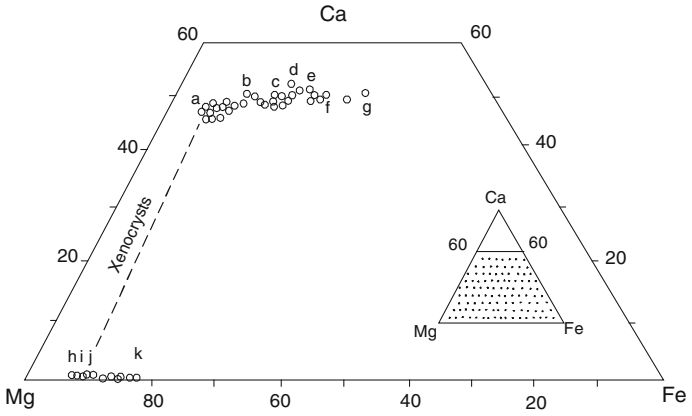

Fig. 2.6 Clinopyroxene and olivine compositions from Brown Leucitic Tuff samples plotted on to the lower portion of the pyroxene quadrilateral (mol %). Letters a–g and h–k indicate analyses of clinopyroxenes and olivine respectively (after Luhr and Giannetti 1987)

the Brown Leucite Tuffs also contain diopside aggregates (Fig. 2.6). The range of salite composition is as follows: $Ca_{49–51}Mg_{31–34}Fe_{16–19}$, whereas, diopside composition plots near $Ca_{47}Mg_{47}Fe_6$.

High K-series rocks (leucite basanite, leucitite, tephritic leucitite, and leucite phonolite) of Vulsini are characterised by pyroxenes, ranging in composition from diopside to salite. The compositional plot of clinopyroxenes from leucite phonolites, trachyte and tephritic leucitites is shown in Fig. 2.6a–c. These pyroxenes also contain more than enough Al to balance silica deficiency in the tetrahedral site, and substitutional relation is of the following type: $Mg^{2+} + Si^{4+} \approx Al^{3+} + Al^{3+}$. In addition to the $CaAl_2SiO_6$ molecule, the pyroxenes also contain $CaFe^{3+}AlSiO_6$ (ferri-Tschermak's component). The pyroxenes from leucite phonolites and trachytes (Fig. 2.7) do not show discontinuous zoning like the ones from tephritic leucitites.

The presence of two types of pyroxenes such as salite and diopside in some Vulsini lavas have been ascribed to variation in $f(H_2O)$ and $f(O_2)$ conditions in the same magma chamber by Luhr and Giannetti. Barton et al. (1982) however, suggested an alternate mechanism for the occurrence of diopside and salite in the same lava flow. According to them this may indicate mixing of two different types of magmas, each characterised by two different types of clinopyroxenes. High pressure of equilibration may be the reason for higher concentration of Na and Al^{vi} in pyroxenes (Thompson 1977) from Alban Hills leucitites. Pyroxenes from Vulsini tephrites and leucitites however, show that diopsides or salites are poor in Na. Clinopyroxenes from leucite-bearing rocks of Latera Caldera (Turbeville 1993) are also either diopside or salite. Dark green salite phenocrysts with similar Ti and Fe contents appear as phenocrysts (Table 2.4). Estimates based on cation deficiency shows that diopside crystals are low in acmite and Ti-bearing components, whereas the content of Tschermak's molecule is lower in the fassaites. The groundmass

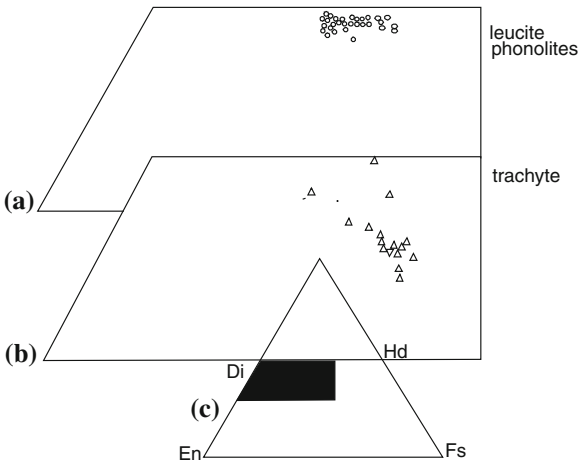

Fig. 2.7 A compositional plot of clinopyroxenes from Vulsini, **a** leucite phonolite, **b** trachyte, and **c** a plot of clinopyroxenes from Vulsini rocks in a pyroxene quadrilateral (after Barton et al. 1982)

pyroxenes in pumice and scoria fragments are salites with consistently higher Ti and Al than coexisting phenocrysts. The larger pyroxene crystals exhibit weak sector or patchy zoning and rarely concentric zoning. Many diopside crystals with fluid inclusions are deeply embayed in dark brown glassy groundmass.

Zoning in clinopyroxene is common in Vico lavas (Perini and Conticelli 2002). The pyroxenes are ubiquitous micro-phenocrystal phase in Vico lavas (Cundari 1975), and sometimes they may be 1/2 cm long along the c-axis. In a conventional plot of Ca–Mg–[Fe(total) + Mn], pyroxene compositions plot within the salite domain, and display a general Fe-enrichment trend parallel to the diopside-hedenbergite join. The distribution of Ti, relative to Al in co-existing core and rim compositions generally show contrasting trends, suggesting complex history of multiple equilibration in the pyroxene-liquid relationship. This may be influenced by temperature and/or f(H_2O) fluctuation during the crystallization of pyroxene, which contains up to 6.91 mol% $CaFeSi_2O_6$, variable amounts of $CaAl_2SiO_6$ (5.7–13.9 mol%), small amounts of acmite (1.2–3.8 mol%) and up to 2.5 mol% $CaTiAl_2O_6$ molecule in solid solution.

Clinopyroxenes from leucite tehprites, phonotephrites, phonolites and foidites from Alban Hills (Italy) are mainly phenocrysts in the post-caldera samples (Aurisicchio et al. 1988). The phenocrysts are of two distinct types: (1) normally zoned variety exhibiting green to colourless core and dark green rim, containing inclusions of opaques and (2) the reversely zoned crystals displaying a green core encircled by a light green rim. The composition of phenocrysts with light green to colourless pyroxene displays enrichment of Al, Fe_t and Ti form the core to the rim and concomitant depletion in Mg and Si. In the reversely-zoned crystals, a rim is characterised by an increase of Si and Mg and depletion of Al, Fe_t and Ti. In a conventional pyroxene quadrilateral, core compositions plot within the diopside field or above the diopside-hedenbergite join. Cores of clinopyroxenes display reverse zoning. The pyroxenes are of two different varieties (either diopside or fassite). The K-rich rocks of Hoch Eifel (Germany) contain fassites (Huckenholz 1973). Duda and Schminke (1985) thought

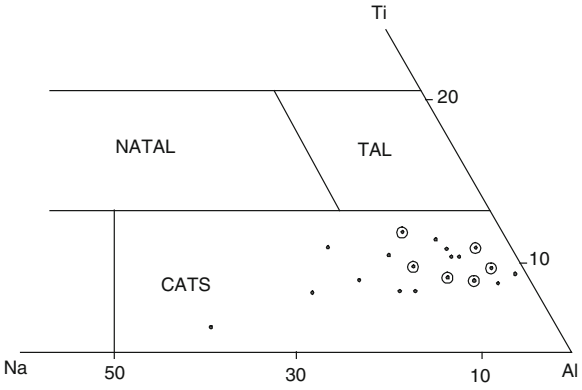

Fig. 2.8 A plot of bulk composition of pyroxenes from Alban Hills in a Na–Al–Ti diagram. The dominant core composition of clinopyroxene is plotted here. In this figure NATAL, TAL and CATAS denotes Na–Al–Ti-rich, Ti–Al-enriched and Ca-Tschermak's molecule respectively (after Aurisicchio et al. 1988)

that the green core pyroxenes from the Eifel region is related to chrome content and their crystallization was associated with polybaric differentiation of alkali basalt magma.

The dominant core composition of clinopyroxenes from Alban Hills is plotted in Fig. 2.8. In this figure NATAL, TAL and CATS denote enrichment in Na, Al (NATAL); Ti, Al (TAL); and Ca-Tschermak's molecules (CATS), respectively. In case of clinopyroxenes from the Alban Hills, Fe^{3+} is the dominant cation in the M_1 site. The ferri-Tschermak's molecules, in fassitic pyroxenes, is higher in the Al^{iv} content in comparison with diopsidic pyroxenes. Aurisicchio et al. found that the Cr content of clinopyroxenes is highly variable. It is particularly high in cores of the diopside phenocrysts ranging from 0.31 to 0.92 and sometimes reaching a value as high as 1.04 % in megacrysts. In the rims, Cr_2O_3 contents could be as high as 0.61 wt%. The TiO_2 content values in the cores of some of the pyroxenes is as high as 0.98–2.58 wt%. In the rim of the same crystal, the TiO_2 content varies between 0.84 and 2.54 wt%, respectively.

2.5 Mica

Lamproites constitute 15–30 vol% of tri-octahedral mica (Wagner and Valde 1986). Some of the micas are authigenic, whereas others are xenocrysts derived from the mantle. Large phlogopites sometimes, occur either as cores of complex micas or may serve as nuclei for crystallization of other micas. Sometimes, cores show that the TiO_2 content is around 2 wt%, surrounded by phlogopite having higher Ti, Fe and lower Al than the cores. Typical lamproitic micas have Fe/(Fe + Mg) ratio always >0.30, with concentric zoning. They show increase in Ti and Fe contents

and a concomitant decrease in Al from the centre to the edge. They are characterised by deficit in the tetrahedral site [e.g. (Si + Al + Cr) < 4 atoms].

The presence of Fe^{3+} in the tetrahedral sites is well-established. Tetra-ferriphlogopite is not only found in nature, but has also been synthesised. In these micas, Si^{4+} and Mg^{2+} can substitute for 2 Al^{3+} in the tetrahedral site (Seifert and Schreyer 1971). The presence of tetrahedral Mg in micas from Smoky Butte lamproites has been demonstrated by Robert (1981). He further showed that in such micas Ti is exclusively located on the octahedral sites.

Different types of substitution in micas have been suggested by different mineralogists as summarised by Wagner and Velde (1986):

$$2\,\mathrm{Mg} = \mathrm{Ti} + \square \quad \text{Forbes and Flower (1974)} \tag{2.1}$$

$$3\,\mathrm{Mg} = \mathrm{Ti} + \mathrm{Ba} + \square \quad \text{Velde (1979)} \tag{2.2}$$

$$\mathrm{Mg} + 2\mathrm{Si} = \mathrm{Ti} + 2\mathrm{Al} \quad \text{Robert (1976).} \tag{2.3}$$

$$\mathrm{Mg} + \mathrm{Si} = \mathrm{Ti} + \mathrm{Mg} \quad \text{Robert (1976), and} \tag{2.4}$$

$$\mathrm{Mg} + 2\mathrm{OH} = \mathrm{Ti} + 2\mathrm{O}\ [\text{Arima and Edgar (1980)}] \tag{2.5}$$

The substitution of type (2.1) can be demonstrated in Fig. 2.9a and b, where Ti has been related to the total number of cations. In this substitution it has been assumed that both the tetrahedral and interlayer sites are filled, and no Fe^{3+} is present in the structure. Authigenic micas in lamproites differ from phlogopites from ultrabasic xenoliths by their higher TiO_2 contents, but xenocrystal micas are found to be similar even in their trace element contents with phlogopites from peridotites.

The micas of wyomingite and olivine orendites (Leucite Hills, U.S.A.) have cores generally enriched in Al_2O_3 and impoverished in TiO_2 than those from the micas of madupites (Kuehner et al. 1981). In comparison to phlogopites from madupites and olivine orendites, those from wyomingites have higher Cr_2O_3 contents. The phlogopite cores from the olivine orendites are enriched in Ti, Ba, Al and Fe and depleted in Mg and Si in contrast to the microphenocrystal phlogopites of the same rock type (Table 2.5).

The Highwood Mountains minettes have phlogopite phenocrysts (up to 10 cm long) characterised by high Fe/(Mg + Fe) ratio (0.1–0.2) with Cr_2O_3 content ranging up to 2.2 wt%. Biotite micro-phenocrysts in mafic phonolites from the same locality have Fe/(Mg + Fe) ratio <0.3, but are more enriched in Ti, Fe, Mg, Ca, Ba, Na and F relative to the phlogopites. As a matter of fact, some of the biotites have the BaO content as high as 7.5 wt% with (Al + Si) <0.8 per 22 oxygen.

The biotites (up to 4 mm long) of the Brown Leucitic Tuffs of Roccamonfina (Italy) have apatite inclusions with Fe/(Mg + Fe) ratio varying between 0.38 and 0.36. In CaO-poor but Fe-rich samples, this ratio is as low as 0.60 (Luhr and Giannetti 1987).

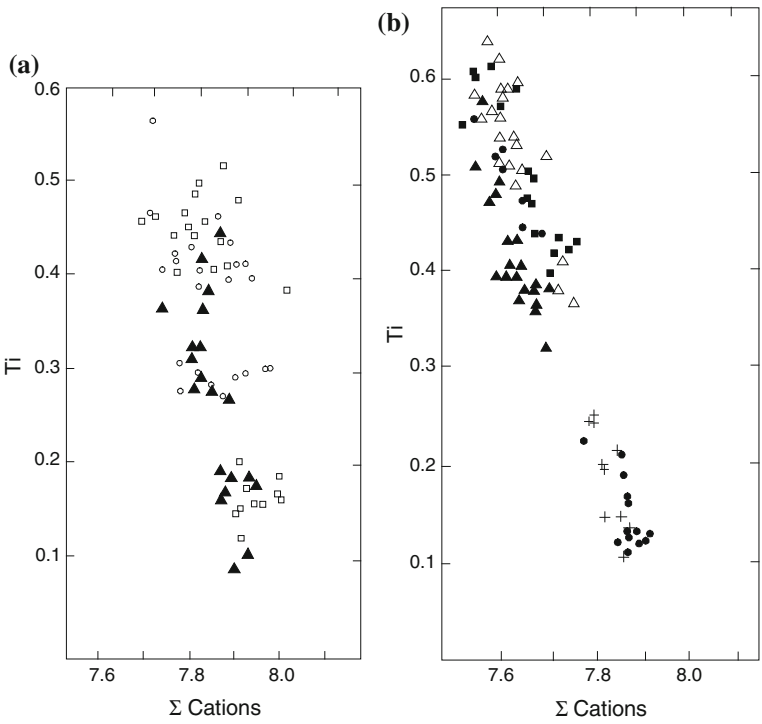

Fig. 2.9 **a** The distribution of Ti and the sum of cations in phlogopite from 3 specimens. *Open squares*: Shiprock lamproite, New Mexico; *open circles*: wolgidite, Mount North, West Kimberley, Australia; *solid stars*: Sisco lampriote, Corsica. **b** The distribution of Ti and the sum of cations in phlogopites from 5 specimens. *Solid triangles*: Concarix lamproites, Corsica; *solid circles*: Calasparra lamproite, Murcia, Spain; *solid squares*: lamproites from Jumilla, Murcia, Spain; *asterisk*: lamproites from Barqueros, Murcia, Spain; *open triangles*: Smoky Butte lamproite Montana, U.S.A (after Wagner and Velde 1986)

In an Al_2O_3–TiO_2 plot, the mica from the lamproitic rocks of Smoky Butte was found to have the highest TiO_2 content (Mitchell et al. 1987). Optically zoned micas have in general a trend of increasing TiO_2 coupled with slight decrease in the Al_2O_3 content. In a similar plot of Al_2O_3 versus TiO_2 contents, micas from K-rich rocks of Alto Paranaiba (Brazil), have chemistry similar to those of micas from West Kimberley, Smoky Butte and Leucite Hills (Gibson et al. 1994). Micas occurring in the K-rich dikes of Trace Ranchos, Limeira I, Indaia I and Pantano, are TiO_2-poor tetra-ferriphlogopites. In other intrusives (e.g. Mata do Lenco) phlogopite shows enrichment in TiO_2 from core to the rim. Phlogopites from Bociana intrusives have moderate TiO_2 (4–5 wt%), Al_2O_3 (12–13 wt%) and total FeO (11 wt%) and plot in the same fields as the groundmass micas of madupites of Leucite Hills. The micas of the lavas from Olegario, Serra do Bueno and Corrego Verjao have high TiO_2 (5–7 wt%), moderate Al_2O_3 (7–11 wt%) and FeO (6–9 wt%) contents. These are quite similar to the micas from West Kimberley and Leucite Hills. The phlogopites

Table 2.5 Analyses of phlogopite

	SiO_2	TiO_2	Al_2O_3	Cr_2O_3	FeO_t^a	MnO	MgO	CaO	SrO	BaO	Na_2O	K_2O	Cl	F	-F = O	Total
1	34.70	6.15	15.90		7.99	0.15	18.20	0.10		3.27	0.12	9.00				95.58
2	39.70	2.83	13.60	0.37	5.71	0.03	22.10	0.04		0.45	0.60	9.52	0.01	3.76	1.58	100.3
3	40.20	2.06	13.50	0.85	4.42	0.02	22.60	0.05		0.41	0.61	9.77		3.56	1.50	96.55
4	39.30	2.40	14.50	0.43	4.06	0.06	22.40	0.06		1.25	0.55	9.71	0.01	3.69	1.55	96.87
5	35.27	4.14	15.07		15.24	0.17	14.60	0.13	0.15	0.49	0.29	9.55		0.70	0.29	96.09
6	35.61	3.97	15.30		15.42	0.18	15.10	0.04		0.09	0.33	9.68		0.50	0.21	96.43
7	35.27	5.39	14.87		16.38	0.25	13.96	0.31			0.31	9.81			0.21	96.48
8	36.01	6.16	16.11		12.51	0.18	15.82	0.05			0.68	9.14	0.01	0.33		97.00
9	36.70	5.22	15.99		8.14	0.05	19.20				0.72	9.39	0.03	0.17		95.61
10	39.87	4.45	13.57	0.06	11.62	0.20	12.96	0.79			2.57	9.93	0.03	0.08		96.13
11	39.90	1.78	12.39		6.62	0.10	22.43				0.43	10.30				93.95
12	37.94	8.41	10.11		8.07	0.08	18.41				0.15	9.87	0.08	0.25		93.37
13	36.44	3.86	14.51		15.99	0.48	15.44				0.49	9.42				96.63
14	39.62	8.12	10.07		7.07		23.10					8.92				96.90
15	39.40	5.69	9.44		6.15	0.08	25.79					9.36				95.91
16	40.18	2.10	12.76		3.02		27.58					9.15				94.79
17	38.99	8.43	8.20		7.65	0.03	19.31	0.60		1.85	0.86	8.75				96.01
18	39.62	8.12	10.07		7.07		23.10					8.92				96.90
19	39.40	5.69	9.44		6.15	0.08	25.79					9.36				95.91
20	40.18	2.10	12.76		3.02		27.58					9.15				94.79

(continued)

Table 2.5 (continued)

	SiO_2	TiO_2	Al_2O_3	Cr_2O_3	FeO_t^a	MnO	MgO	CaO	SrO	BaO	Na_2O	K_2O	Cl	F	-F = O	Total
21	42.14	2.06	11.38	0.08	3.00		25.84			0.33		10.41				95.24
22	41.28	2.15	11.89	0.89	2.96	0.07	24.85			0.52	0.13	10.61				95.35
23	42.46	3.70	7.72		5.64	0.02	23.56			1.47	0.62	10.16				95.35
24	39.94	3.90	12.41	1.33	3.07	0.01	24.44			0.05	0.01	10.24				95.40
25	38.68	11.19	8.79	0.03	11.49	0.08	16.24			2.11	0.46	8.30				97.37
26	39.74	7.04	11.27	0.76	3.88	0.02	22.12			1.11	0.10	9.63				95.67
27	38.60	3.14	13.13	1.32	4.79		23.26			0.34	0.60	10.74				95.92

[a] FeO_t represents total FeO + Fe_2O_3 content

1 Mica from a leucitite, Gaussberg, Antarctica (Sheraton and Cundari 1980)
2–4 Phlogopites from ultrapotassic rocks of Sierra Nevada (van Kooten 1980)
5–7 Phlogopites from leucitic tuffs, Roccamonfina Volcano, Italy (Luhr and Giannetti 1987)
8–10 Phlogopites from a leucite-bearing rocks of Laacher See, Germany (Duda and Schminke 1978)
11 Phlogopite from a phonotephrite, Alban Hills, Italy (Aurisicchio et al. 1988)
12 Phlogopite from a lamproitic rock Damodar Valley coal field (Gupta et al. 1983)
13 Phlogopite from a potassic rock occurring at Vulsini volcanic field, Italy (Francalanci et al. 1987)
14–16 Phlogopites from ultrapotassic rocks of Spain (Lopez Ruiz and Badiola 1980)
17 Phlogopite from a K-rich lamproite of Spain (Borley 1967)
18–20 Phlogopites from lamproitic rocks, Southern Spain (Lopez-Ruiz and Badiola 1980)
21 Phlogopite from an olivine orendite, South Table Mountain, Leucite Hills, Wyoming (Kuehner et al. 1981)
22 Phlogopite from a wyomingite, Zirkel Mesa, core of phlogopite grain, Leucite Hills, Wyoming (Kuehner et al. 1981)
23 Phlogopite from a madupite, Pilot Butte, Leucite Hills, Wyoming (Kuehner et al. 1981)
24 Phlogopite from a Calasparra lamproite, Murcia, Spain (Wagner and Velde 1986)
25 Phlogopite from a jumillite lamproite, Murcia, Spain (Wagner and Velde 1986)
26 Phlogopite from a lampoite, Smoky Butte, Montana, U.S.A. (Wagner and Velde 1986)
27 Analysis of a phlogopite from the Shiprock dyke lamproite, New Mexico, U.S.A. (Wagner and Velde 1986)

from the Alto Paranaiba Igneous Province do not show any overall peculiarity, but have chemistry similar to those of kimberlites and lamproites in terms of their TiO_2 and Al_2O_3 contents.

The solubility of TiO_2 in phlogopites crystallizing in the simplified system, $K_2Mg_6Al_2Si_6O_{20}(OH)_4$–$K_2Mg_4TiAl_2Si_6O_{20}(OH)_4$–$K_2Mg_5TiAl_4Si_4O_{20}(OH)_4$ was determined at variable pressures between 1 and 3 GPa and 825–1300 °C, under a condition of $P(H_2O) < P(Total)$ by Tronnes et al. (1985). They found a complete substitution of the following types: Mg^{VI}, $2Si^{IV} \approx Ti^{IV}$, $2Al^{IV}$ and $2Mg^{VI} \approx Ti^{IV}$ in phlogopite. They tried four sets of experiments with Ti-phlogopite containing 7.1, 6.3, 4.8 and 2.4 wt% TiO_2 at variable temperatures. Their study on phlogopite co-existing with rutile and vapour indicates that Ti content of phlogopite increases with temperature at a given pressure. Their investigation on phlogopite in equilibrium with rutile and a vapour phase shows that it has 7.1 wt% TiO_2 at 1,275 °C or higher temperatures under 3 GPa. The same Ti-phlogopite is stable under following conditions: 1,110 °C and 2 GPa, above 1,025 °C and 1 GPa, above 1,275 °C and 3 GPa, above 1,110 °C and 2 GPa and finally at 1,025 °C and 1 GPa. The Ti-phlogopite breaks down to rutile and a vapour phase at lower temperatures.

The Orciatico lamproites (Conticelli et al. 1992) have micas, with fairly homogeneous chemistry. They have high TiO_2 (7–8 wt%), BaO (0.2–1.8 wt%) and MgO (16–17 wt%) content and low abundance of SiO_2 (37–40 %) and Cr_2O_3 (0.01–0.06 %). The (Si + Al) and (Na + K) are insufficient to fill the tetrahedral site (2.2) and interlayer (W) site, respectively. They suggested that possible substitution as $(Ti^{VI,\ 4+} + Mg^{IV,\ 2+}) \approx Mg^{IV,\ 2+} + Si^{IV,\ 4+}$ is more realistic (Robert 1976). They noted positive correlation between Al and Ti and following type of substitution involving $(Ba^{2+} + Al^{3+})$ and $(K^+ + Si^{4+})$. The micas occurring in lamproites from Monticatini Valdi Cecina (Italy) are strongly zoned and have wide compositional range of TiO_2 (2–7 %), MgO (15–24 %) and FeO (4–13 %). In these micas, they noted following type of substitution: $2Mg^{IV,\ 2+} \approx Ti^{IV,\ 4+}$ (Forbes and Flowers 1974). Such a substitution as $Mg^{IV,\ 2+} + 2Si^{IV,\ 4+} \approx Ti^{VI,\ 4+} + 2Al^{VI,\ 4+}$ (Arima and Edgar 1981) is also noted. The variable K/Al ratio in these micas probably reflect f (O_2) variation (Foley 1989). Biotite occurs rarely as phenocrysts in pumice clasts and is intergrown within plagioclase and pyroxene. Isolated crystals are replaced by magnetite. Altered biotite phenocrysts have Fe/(Mg + Fe) ratio varying between 0.42 and 0.21 and F content is as high as 1.14 wt%.

The leucite tephrites and tephritic leucite phonolites from Vico lavas (Cundari 1975) have micas with Fe/Mg ratio >1:2, suggesting that they are phlogopitic. Mica in the groundmass of basic phonolitic leucite tephrite is also within the phlogopite range [(Fe/Mg) ratio = 0.39−0.33]. The pleochroic scheme of mica is as follows: α (pale yellow) < $\beta = \gamma$ (dark brown to greenish brown).

Phenocrystal phlogopites in leucite-bearing lamproitic rocks of Leucite Hills are very common minerals, but they are absent in the groundmass (Carmichael 1967). It occurs as large polysynthetically twinned crystal with evidence of resorption in wyomingites and orendites. Micas often are weakly pleochroic from yellow brown to nearly colourless, but sometimes the core shows more intense pleochroism than the rim and may include spinel. The phlogopites from Wyomingite contain up to

2.46 % F. The high F (2.16 wt%) content has also been found in high K-rich Spanish lamproites. The concentration of Ti is particularly high in phlogopites from leucitic rocks of Australia and Spain in contrast to those from Leucite Hills (Carmichael 1967, Table 2.5).

The Gaussberg leucitites have micas, which are late crystallizing phases (Sheraton and Cundari 1980). They are also titaniferous but high in BaO (1.0 wt%) and similar to those in Smoky Butte (Velde 1975) and West Kimberley (Carmichael 1967), but poorer in Al. There is more Al atom for 22 oxygens, and much of the Ti is assumed to be in the tetrahedral site.

2.6 Amphibole

Cross (1897) reported for the first time unusual pleochroism in amphiboles (lemon yellow to pink or reddish pink) from the lamproitic rocks of Leucite Hills. Similar amphiboles have also been described from the potassic rocks (jumillite) of south-eastern Spain (Wagner and Velde 1986) and West Kimberley, Australia (Jaques et al. 1984). They were originally described as magnophorite, but are essentially a variety of K-richterites [(Na, K) Na,Ca $(Mg,Fe^{2+})_5Si_8O_{22}(OH)_2$]. K-richterites belong to the calc-alkaline amphibole group, and have almost one Fe^{2+} atom in the C-site. Richterites found in Shiprock and Sisco lamproites however, are richer in iron varying between Mg_2Fe_3 and Mg_3Fe_2 (Wagner and Velde 1986). The A site (Na + K) is overfilled and the tetrahedral sites are underfilled [(Si + Al) < 8)]. The remaining tetrahedral site presumably contains Fe^{3+}, but in Calasparra lamproites, even after assigning Si, Al and Fe^{3+}, the tetrahedral site remains incomplete.

The Ti content of richterites in lamproitic rocks are usually high in kaersutites (Yagi et al. 1975), and the average is around 2 wt%, but up to 9 wt% is noted in Moon Canyon lamproites (Wagner and Valde 1986). In amphiboles with high Ti concentration (Cancarix, Calasparra and Moon Canyon), the presence of titanium creates a vacancy in the structure as can be seen in the diagram representing the variation of Ti versus the sum of cations (Fig. 2.10a and b). The P–T stability of kaersutite has been studied by Merill and Wyllie (1975).

Ti-deficient amphiboles display a negative correlation between the Ti content and number of (Si + Al) ions in the tetrahedral site. There is no relationship however, between Ti contents and sum of cations. There are some amphiboles, which are zoned. For example, the Cancarix (Spain) and Australian lamproites show darker colour towards the rim of the grains, which corresponds to an increase in Ti and Fe^{2+} and decrease in Mg. The observation may be related to the following types of substitution: ($\square$ + Ti + Fe^{2+}) ≈ 3 Mg. Slightly Ti-rich K-richterite coexists with phlogopite, clino-pyroxene and leucite in the leucitites of New South Wales (Cundari 1973). The formula of these amphiboles is as follows: $(Na,K)_{2.0}Ca_{0.8–0.9}(Mg, Fe^{2+}, Mn, Fe^{3+}Ti)_5(Si, Al, Ti)_8O_{22}(OH)_2$. In comparison to the richterites occurring in West Kimberley rocks, those present in the leucitites from New South Wales are more sodium rich.

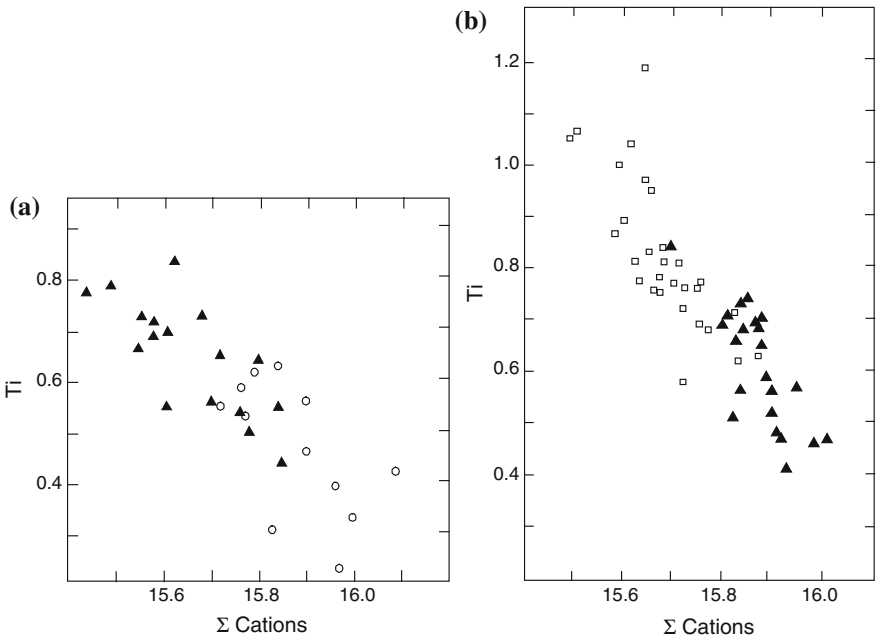

Fig. 2.10 **a** The distribution of Ti and the sum of cations in richterites from Cancalite, Cancarix, Albacete, Spain (*solid triangles*); and richterites, Calasparra lamproites from Murcia, Spain (*open circles*). **b** The distribution of Ti and sum of cations in richterite from Moon Canyon, lamproite Utah (*open squares*) and richterite from jumillite, Smoky Butte, Montana (*solid triangles*) (after Wagner and Velde 1986)

Leucite-bearing tephrites and basanites of West Eifel (Duda and Schminke 1978, Table 2.6) also contain brown yellow amphiboles. The Ti-content of these amphiboles is <5 wt% and they are kaersutites. They have higher F content in the rim compared to that in the core.

Leucite-bearing tephrites and basanites of West Eifel (Duda and Schminke 1978, Table 2.6) also contain brown yellow amphiboles. The Ti-content of these amphiboles is <5 wt% and they are kaersutites. They have higher F content in the rim compared to that in the core.

Tipolo et al. (2003) studied Solid/liquid partition coefficients for large ion lithophile elements (Ba, Rb, Sr), high field strength elements (Zr, Hf, Nb, Ta, Ti), rare earth elements (La-Yb), Pb, Th, U and selected transition elements (Sc, V) were determined by means of Secondary Ion Mass Spectrometry on potassic-richterites synthesised at upper mantle conditions (P = 1.4 GPa and T = 850–1020 °C) from silica-rich lamproites. They observed that most trace elements display an incompatible behaviour in potassic-richterites; only Sr, Ti, Sc and V show strong positive anomalies in the partitioning pattern. When (S/L)-D for potassic-richterites are compared with those for calcic amphiboles (pargasites and kaersutites) several differences become evident. In general, D-S/L are lower in

Table 2.6 Analyses of K-richterite from ultrapotassic rocks

	SiO_2	TiO_2	Al_2O_3	FeO[a]	Fe_2O_3	MgO	MnO	CaO	Na_2O	K_2O	Cr_2O_3	BaO	F	Cl	SrO	Total
1	53.76	5.48	0.61	4.33		18.58		6.16	3.92	4.26						97.10
2	54.20	5.95	1.76	5.82		17.01		4.91	4.37	4.67						98.69
3	54.70	5.90	0.59	5.40		15.55		4.67	4.56	4.54						95.91
4	53.20	5.20	1.10	5.70		17.3	0.13	5.20	5.10	4.40		0.20			0.38	97.91
5	52.70	3.72	1.21	3.23	0.94	18.76	0.09	8.48	4.05	4.00		0.80				97.98
6	38.33	4.45	14.17		10.87	12.38	0.22	11.64	1.94	2.16	0.06					96.22
7	39.87	4.45	13.57		11.62	12.96	0.2	11.79	2.53	1.93	0.06		0.08	0.03		99.09
8	38.84	4.69	13.93		12.23	12.54	0.16	11.73	2.34	1.99			0.24	0.04		98.73
9	52.89	5.14	0.41	4.51		18.65				3.64						96.16
10	54.40	3.81	0.33	7.08		18.58	0.09			2.51						97.65
11	48.85	3.23	1.62	17.85		12.36	0.21			1.52						95.89
12	51.24	6.34	0.53	5.45		18.12	0.05			5.55						97.60
13	54.50	1.64	0.93	8.05		18.13	0.11			1.32						96.42

[a] If only FeO values are given, then they indicate total FeO + Fe_2O_3 contents

1–3 K-richterite from lamproitic rocks of Smoky Bute (Mitchell et al. 1987)

4–5 K-richterite form ultrapotassic rocks of Spain (Lopez-Ruiz and Badiola 1980)

7–8 K-richterite from leucite tephrite, Laacher see (Duda and Schminke 1978)

9 Analyses of richterite from Cancarix lamproite, Spain (Wagner and Velde 1986)

10 Analyses of richterite from Barquerox lamproite, Murcia, Spain (Wagner and Velde 1986)

11 Analyses of richterite from Shiprock dyke lamproite, New Mexico, U.S.A. (Wagner and Velde 1986)

12 Analyses of richterite from Mount North lamproite, West Kimberley, Australia (Wagner and Velde 1986)

13 Analyses of richterite from Orciatico lamproite Pisa, Italy (Wagner and Velde 1986)

potassic-richterites; also, different partitioning patterns are apparent for REE and LIL elements, where S, L and D refers to solid, liquid and distribution coefficient. These differences discussed by Tipolo et al. (2003) are described in terms of the distinct crystal-chemical behaviour of the involved amphibole-end-members, with particular emphasis to the available charge balance mechanisms and to the site dimensional constraints resulting in incorporation of trace elements in various sites.

The distinct partitioning behaviours of trace elements in potassic-richterites and pargasites and kaersutites imply that melts produced from amphiboles-bearing sources may differ markedly depending on the type of amphiboles crystallised. The new partitioning data may be used to determine the role of potassic-richterite in its principal modes of occurrence, namely in lamproites, in peralkaline ultramafic veins in the lithospheric mantle, and in the deeper parts of subduction zones.

2.7 Olivine

Olivine is an important mineral in leucite-bearing basanites, lamproites, minettes (with high mg-numbers), katungite and mafurites, where it occurs as phenocrysts ($Fo_{84–92}$) and megacrysts ($Fo_{88–92}$, Table 2.7). In the potassic rocks of Alto Paranaiba Igneous Province (Gibson et al. 1995), olivine exhibits slight compositional variation, whereas olivine inclusions show compositional zonation ($Fo_{84–87}$).

Both phenocrystal and groundmass olivines are present in olivine orendites (Kuehner et al. 1981) from Spring Boat, North Table Mountain and South Table Mountain (Leucite Hills, Wyoming, U.S.A., Table 2.7). Leucitites occurring in New South Wales, Australia (Cundari 1973), are characterised by olivine ($Fo_{93–79}$) phenocrysts (0.3–3.0 mm along c-axis, Table 2.7). Iddingsites (pseudomorph after olivine) are common.

Orciatico lamproites (Italy) have olivines having wide range of compositions (Fo_{74}–Fo_{92}) with no chemical zonation. The CaO and MnO content of the olivines increase systematically with decrease in the forsterite content. Large rounded crystals with kink banding are very much common in the Orciatico lamproite.

Brown Leucitic Tuffs from Latera Caldera (Luhr and Giannetti 1987; Table 2.7) are characterised by the presence of forsteritic olivines ($Fo_{82–91}$). The rims and fractures within olivines are filled by iddingsites. Diopside crystals often form clusters with olivines, which are probably xenocrysts. Olivine occurs in the basanites of Mt. Vulture complexes. It is usually found as a phenocryst, intergrown with diopside. This phase however, does not show any reaction rim. The olivine grains have narrow compositional range ($Fo_{89–88}$, Table 2.7).

The leucite-bearing lavas of EK series from Ringgit–Beser complex, East Java (Edwards et al. 1994) contain phenocrystal forsteritic olivine ($Fo_{91–92}$). They have quenched skeletal textures and show alteration to iddingsite. Olivine phenocrysts (Table 2.7) in the minettes from Bearpaw Mountains, Montana (Macdonald et al. 1992) are usually idiomorphic and 3 mm long. Some crystals show resorption. Normal zoning towards Fe, Mn and depletion in Ni is quite common. Olivine

Table 2.7 Analyses of olivine from K-rich localities

	SiO_2	FeO	MnO	MgO	CaO	NiO	Total
1	41.25	8.00	0.09	49.83	0.10	0.62	99.89
2	40.20	9.58	0.09	49.86	0.16	0.43	100.32
3	41.07	11.41	0.14	47.25	0.16	0.33	100.36
4	40.80	8.02	0.05	50.10	0.10	0.52	99.59
5	40.30	15.40	0.18	44.00	0.16	0.18	100.22
6	40.70	10.20	0.05	49.00	0.12	0.12	100.19
7	40.17	9.35	0.18	49.30	0.42		99.42
8	40.53	10.93	0.21	47.75	0.43		99.85
9	39.46	16.17	0.27	43.55	0.23		99.68
10	41.84	7.14		50.82	0.03	0.08	99.91
11	40.41	9.73	0.33	48.77	0.15	0.18	99.57
12	40.71	9.85	0.38	49.18	0.11	0.21	100.44
13	38.55	12.27	0.61	47.56	0.62	0.25	99.86
14	39.00	18.70	0.43	41.10	0.29	0.15	99.670
15	39.30	18.60	0.38	40.90	0.42	0.10	99.70
16	40.00	11.60	0.15	47.20	0.24	0.19	99.38
17	37.80	25.30	0.53	35.80	0.57		100.00

(continued)

Table 2.7 (continued)

	SiO_2	FeO	MnO	MgO	CaO	NiO	Total
18	37.39	32.60	0.92	28.50	0.49		99.90
19	37.29	31.50	0.76	29.90	0.55		100.00
20	40.30	10.50	0.19	48.20	0.33	0.38	99.93
21	39.00–40.80	9.50–11.20	0.14–0.26	46.90–49.90	0.18–1.00	0.16–0.62	
22	40.45	11.41	0.12	47.31	0.41		99.70
23	40.84	10.88	0.22	48.31	0.43		100.68

1–3 Olivines from lamproites of Smoky Butte, U.S.A. (Mitchell et al. 1987)
4–6 Olivines from ultrapotassic rocks of Sierra Nevada, U.S.A. (van Kooten 1980)
7–9 Olivines from leucitic tuffs, Roccamonfina, Italy (Luhr and Giannetti 1987)
10 Olivine from an orendite (SK 36), South Table Mt., Olivine rimmed by phlogopite, average of four analyses (Kuehner et al. 1981)
11 Olivine from an orendite (SK 35), North Table Mt., groundmass olivine, average of two analyses (Kuehner et al. 1981)
12 Olivine from an orendite (SK 36), groundmass olivine, average of two analyses (Kuehner et al. 1981)
13 Olivine from an orendite (SK-37), Spring Butte, single analysis of groundmass olvine (Kuehner et al. 1981)
14–16 Olivines from leucitites, New South Wales (Cundari 1973)
17–19 Olivines from leucite basanites, Vesuvius, Italy (Baldridge et al. 1981)
20 Mean of 12 olivine analyses, leucitites from Gaussberg, Antarctica (Sheraton and Cundari 1980); also contains 0.03 wt% Cr_2O_3*21* Range of olivine analyses of leucitites from Gaussberg, Antarctica (Sheraton and Cundari 1980)
22–23 Olivines from the Mt. Vulture volcanic complex, Italy (Melluso et al. 1996)

crystals show overall change in composition from Mg-rich core towards Fe-enriched rim, as bulk rocks become more evolved. In some crystals compositional range of olivine is found to vary from $Fo_{93.5–87.5}$ to a larger range $Fo_{93.4–69.7}$ or $Fo_{91.0–77.4}$, suggesting that olivine could not have reached equilibrium with the host magma. Macdonald et al. (1992) considered that this diverse olivine population probably resulted from magma mixing.

Gaussburg olivine leucitites have forsteritic olivines ($Fo_{91–92}$) (Table 2.7), and as expected is high in NiO (0.2–0.6 wt%) and CaO (0.2–1.0 wt%), consistent with crystallization from a Mg-rich liquid under low pressure volcanic regime. In the Lyzhnaya pipe of Aldan (Russia), lamproitic pipes consist of forsteritic olivine (10–20 vol%), diopside and phlogopite. The fine-grained groundmass comprises microlites of diopside, phlogopite and K-feldspar. The Ryabinovaya pipe is a olivine-diopside lamproite, where forsteritic olivine ($Fo_{92–94}$) with up to 0.5 wt% NiO constitutes 15–25 vol% of the rock. Chromite inclusions (Cr_2O_3 up to 61 vol%) are present in these rocks.

2.8 Nepheline

It has a cubic symmetry at or above 1,254 °C (Bowen 1912), but hexagonal symmetry at low temperatures under atmospheric pressure. The cubic phase is called carnegieite. Nepheline usually contains albite; and at 800 °C the maximum amount of albite incorporated in nepheline is about 33 wt% (Greig and Barth 1938) under one atmospheric pressure. It has also an extensive solid solution relationship with kalsilite at 0.5 GPa (Zeng and MacKenzie 1984; Fig. 2.11). The system has a truncated solvus with a maximum temperature at 800 °C and $Ne_{30}Ks_{70}$. Phase relations of the join nepheline-kalsilite have also being studied by Gupta et al. (2010). Their isobaric diagram at 2 GPa and variable temperatures is shown in Fig. 2.12.

Holmes and Harwood (1937, p. 37) described nepheline-bearing leucitites from the potassium-rich volcanic fields of following localities in Uganda: Mabunga,

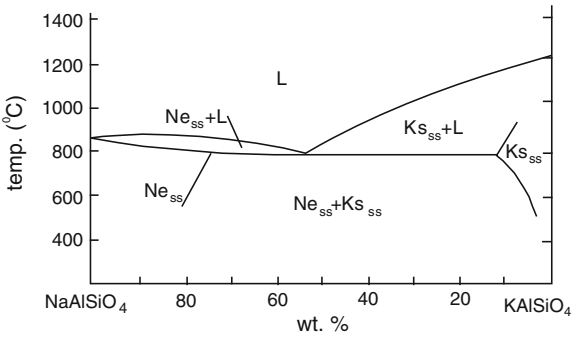

Fig. 2.11 Phase relations in the system nepheline-kalsilite at 0.5 GPa (after Zeng and MacKenzie 1984)

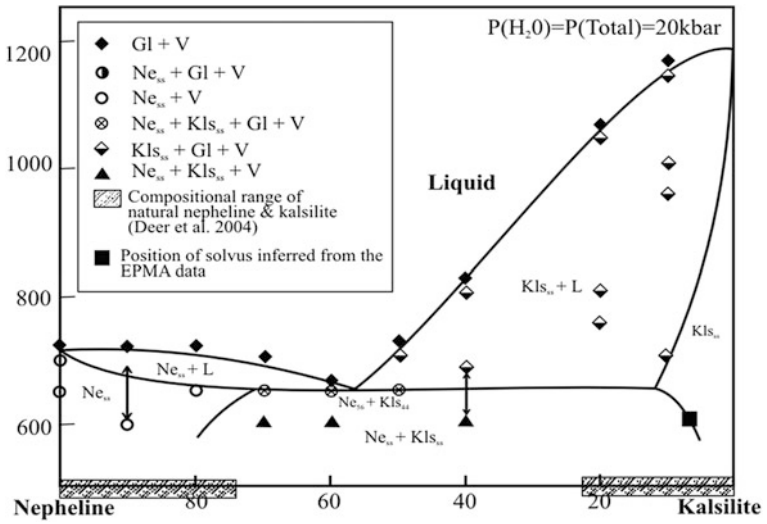

Fig. 2.12 Phase relations along the join nepheline—kalsilite determined at 2 GPa [$P(H_2O) = P$ (Total)] and various temperatures. The *solvus* has been inferred from EPMA data for *subsolidus* runs (after Gupta et al. 2010)

Duzakara, Bunagana and Hyamachunchu. Nepheline together with melilite and leucite has also been reported from the Fort Portal area of Toro-Ankole by Holmes and Harwood (1932, p. 379). It occurs in lavas of Lake Kivu (Bowen and Ellestad 1937). Nepheline-bearing rocks are also present at Villa Senni, Italy.

Nepheline occurs as a groundmass phase in Roccamonfina leucite phonolite lavas (Melluso et al. 1996). Leucite-rich phonolitic tephrite occurs south of Lake Barciano (Sabatini district), and are characterised by nepheline in the groundmass.

Mt. Vulture volcanics (Table 2.8) contain nephelines with excess silica. For example, in Prete della Schimmia, a nepheline crystal ($Ne_{70}Ks_{25}Q_5$) with low CaO content up to 2 wt%) have been described by Melluso et al. (1996). The SrO content of these nephelines is low.

Melilite-bearing foidite occurring south of Caterira, comprises nephelines, which are more Ca-rich with values ranging from 3 to 7 wt%. One particular sample yielded a value of 8.83 wt%, corresponding to a normative anorthite content of 17 %. These nephelines are lower in K contents compared to that of the haüyne-nephelinites and melilitites. Melluso et al. (1996) thought that such high CaO contents have never been reported earlier. They further observed that nephelines from Toppo S. Paolo phonolite have high amount of silica ($Ne_{75}Ks_{13}Qz_{12}$) and plot near Barth's compositional trend: $(K_2Na_6Al_8Si_8O_{32} \rightarrow \square_2Na_6Al_6Si_{10}O_{32}$ (Dollase and Thomas 1978).

Nepheline is a rare euhedral mineral in the leucitites from New South Wales, Australia. These nephelines ($\in$ = 1.530–1.537; ω = 1.534–1.541) are characterised by excess SiO_2 (Cundari 1973; Table 2.8). It occurs as euhedral crystal in the

Table 2.8 Analyses of nephelines from K-rich mafic and ultramafic lavas

	SiO_2	TiO_2	Al_2O_3	Fe_2O_3	FeO[a]	MgO	CaO	SrO	BaO	Na_2O	K_2O	H_2O	Total
1	46.00	0.05	30.10	2.90		0.66	0.06			16.20	4.70		100.67
2	42.80	0.06	32.70	1.70		0.10	0.06			15.70	6.90		100.02
3	42.30		34.00	0.72			2.90			15.10	4.20		99.22
4	45.95		31.31	0.47			0.95	0.03	0.36	17.55	3.88		100.5
5	47.40		31.40	0.82			0.73			16.40	3.20		99.95
6	40.20	0.05	32.51	1.80		0.10	1.44			10.86	12.22	0.20	99.38
7	38.47		30.81	1.63		0.63	0.20			2.09	25.65		99.48
8	38.42	0.05	31.01	1.12			0.03			0.30	28.33	0.67	99.93
9	48.33		31.1		1.06	0.46	0.46			16.04			100.82
10	48.43		30.97		1.08	0.44	0.44			16.03			100.86
11	43.12		33.49		1.23	3.41	3.41	0.24		14.17			100.16
12	42.76		30.01		2.08	8.83	8.83	0.29		12.01			99.33
13	42.77		33.50		1.14	3.72	3.72	0.29		13.56			99.56
14	45.83		32.64	0.49			0.27			17.05	3.73		100.01

(continued)

Table 2.8 (continued)

	SiO_2	TiO_2	Al_2O_3	Fe_2O_3	FeO[a]	MgO	CaO	SrO	BaO	Na_2O	K_2O	H_2O	Total
15	49.27		29.56	0.93			Trace			16.26	3.07		99.09
16	45.59		32.46	0.61			1.22			16.25	3.31		99.44
17	48.23		31.40	0.51			0.77			16.02	3.13		100.06

[a] FeO indicates total FeO + Fe_2O_3 contents

1 Nepheline from a lava flow at Condobolin, New South Wales (Cundari 1973)
2 Nepheline from a lava flow at Cargelligo, New South Wales (Cundari 1973)
3 Nepheline from a leucite-tephrite, Sabatini, Italy (Cundari 1979)
4–5 Nephelines from a lava flow at the Roman province (Baldridge et al. 1981)
6 Nepheline from a potash ankaratrite, Zaire (Sahama and Wilk 1952)
7 Kalsilite from a venanzite, Italy (Bannister et al. 1953)
8 Kalsilite from a K-rich rock at Zaire (Sahama et al. 1956)
9–13 Nephelines from Mt. Vulture volcanic complex (Melluso et al. 1996)
14–15 Nepheline from Portobello (Wilkinson and Hensen 1994)
16–17 Nepheline from Nombi (Wilkinson and Hensen 1994)

groundmass of leucite basanites and tephrites from the Laacher See area, East Eifel, Germany.

The potassic rocks of Ishimskii, Central Kazakistan, are characterised by extrusive and subvolcanic facies rocks containing pseudoleucite phenocrysts in a groundmass comprising microlites of K-feldspar, nepheline, and altered glass. In the pseudoleucite-bearing nepheline syenites from lamproites of Central Asia (42°09′ N, 74°59′ E), nepheline occurs quite commonly.

This mineral (comprising up to 35 vol% of the rock) occurs in the alkali intrusive rocks at Changit (Maimecha Kotui Province, Russia), where it occurs in association with perovskite, aegirine-augite, apatite, K-feldspar and phlogopite.The syenites comprise pseudoleucite (2–6 cm in across) in a matrix of granular nepheline and alkali feldspar. In these rocks pseudoleucite constitutes 30–40 vol% of the rock.

The mineralogy and chemistry of nephelines crystallizing in some alkaline rocks of New South Wales were studied by Wilkinson and Hensel (1994). They noted that except for a few exceptions, the nephelines are Si-rich types, whose Qz (quartz) components exceed those defining the limits of excess SiO_2 in solid solution in the Ne–Ks–Qz–H_2O system at 700 °C and 0.1 GPa P(H_2O). They further established that the nephelines in the basanites show only limited grain-to-grain compositional variation. The nephelines in theralites and tinguaites from the differentiated Square Top intrusion of New South Wales, and in the New Zealand tinguaite however, vary significantly in Ne (nepheline), Ks (kalsilite) and Qz contents even within individual samples. These nephelines may also be strongly zoned. They found that the rims of zoned nephelines are enriched in Si and Fe^{3+}, relative to core compositions. These zoning trends contrast with the compositional trend of successive "bulk" nepheline fractions in the Square Top sequence from thearalite to tinguaite, where Qz content decreases. The nephelines coexist with high-temperature alkali feldspars. Wilkinson and Hensel noted that in the Ne–Ks–Qz system they plot on the Ne-rich side of the Barth compositional join, defined by the omission solid solution series with end-members $K_2Na_6Al_8Si_8O_{32}$ (the Buerger ideal composition; $Ne_{75}Ks_{25}$ mol%) and $\square_2Na_6Al_6Si_{10}O_{32}$ (□ denotes cavity cations vacancy'). The compositions of most natural nephelines are restricted to the field defined by Ne in the Barth join. Compositions more K-rich than the ideal composition are relatively rare, but those lying close to the Ne side of the join are controlled by a number of factors which include the physical conditions attending nepheline crystallization and the chemistry of the alkaline hosts.

2.9 Kalsilite

Hexagonal kalsilite ($KAlSiO_4$) inverts to an orthorhombic variety at 850 °C under atmospheric pressure. The solid solution relationship between kalsilite and nepheline at, 0.5 and 2 GPa are shown respectively in Figs. 2.11 and 2.12. The mineral kaliophilite (another hexagonal polymorph) has a compositional range identical to kalisilite and it may be metastable at room temperature. Kalsilite is a rare mineral in

K-rich volcanic rocks. It has been described form mafuritic rocks of Uganda and also from the Alto Para-naiba igneous province of Brazil. Kalsilite-bearing lava has been described from Mt. Cimini also.

A nepheline-kalsilite-bearing intrusion occurs at Pkhrutskii (Caucasus). This intrusive covers an approximate area of 10 $km^2$and can be classified as a nepheline-kalsilite-bearing monzonite, which locally grades to essexite and fine-grained syenite. The main rock-forming minerals are nepheline, kalsilite, K-feldspar, augite, aegirine-augite and biotite.

A pseudoleucite-bearing alkali syenite occurs at Yaksha, Baikal (Russia). The syenite comprises pseudoleucite (up to 20 vol%) and nepheline. Nepheline-kalsilite intergrowth is often seen in thin section. Locally the syenite grades to kalsilite syenite. This intrusive body constitutes 65–75 % K-feldspar, 3–10 vol% biotite and up to 2 vol% kalsilite.

Predominantly katungites and mafurites have been described from Quaternary volcanic complex at San Venanzo (Perubia Province) and Cupaellow (Rieti province) of Italy, by Gallo et al. (1984). The mafurites are constituted of kalsilite, melilite and pyroxene.

Gittings et al. (1982) described pyroxenites containing an intergrowth of nepheline and kalsilite from Batbjerg complex of Greenland. Kalsilite-bearing ultrapotassic rocks constitute a 350 km long belt trending NE–SW. It is extended from the Derby Mountains of eastern Seward Peninsula to Kobuk-Selawik.

2.10 Analcite

The analcine problem and its impact on the geochemistry of ultrapotassic rocks from Serbia has been discussed by Prelevic et al. (2002). According to them Tertiary ultrapotassic volcanic rocks from Serbia occasionally display low levels of K_2O and K_2O/Na_2O. In these rocks, analcime regularly appears as pseudomorphs after pre-existing leucite microphenocrysts. The process of leucite transformation in Serbian ultrapotassic rocks is very thorough: fresh leucite survives only in ugandites from the Koritnik lava flows as well as in rare inclusions in clinopyroxene. Their study focuses on the impact of "analcimization" on the mineralogy and geochemistry of the Serbian ultrapotassic rocks, using the samples where relecit leucite has been used as a monitor for the process.

Some minettes from Bearpaw Mountains contain as much as 30 vol% of analcite phenocrysts. They often occur as rounded clear grains (2 mm across), but in some cases the crystals are turbid, and low in K_2O content (<1 wt%, Table 2.9), and the total oxide content of analcite is 88–89 wt% with 10 wt% H_2O. The analcites in the minettes are secondary formed by reaction between leucite and a Na-rich fluid (Macdonald et al. 1992).

This mineral occurs as an interstitial phase in the Square Top intrusion. Analcite displays extensive Na, Al ⇔ Si substitution (Wilkinson and Hensel 1994). Their composition extends from analcite to natrolite (slightly more Si-rich than "ideal"

Table 2.9 Analyses of analcite from various ultrapotassic volcanic complexes

	SiO_2	Al_2O_3	Fe_2O_3	FeO[a]	CaO	Na_2O	K_2O	BaO	H_2O	Total
1	55.91	21.64	1.05	0.09	0.19	12.00	0.25		8.50	99.63
2	51.39	23.48	1.55	0.21	0.20	12.78	1.92		8.20	99.73
3	58.43	21.33	0.93		0.05	9.17	0.34			90.25
4	59.05	21.28	1.00		0.05	9.54	0.29			91.21
5	57.70	19.90		0.90	0.16	12.20	0.52			91.38[b]
6	55.66	21.59		1.17	0.23	12.40	0.30			91.35[b]
7	57.57	20.00		0.81	0.20	12.00	0.49			91.07[b]
8	55.86	21.57	0.44	0.02	0.94	12.67	0.66	0.01		92.17
9	54.71	22.90	0.10		Trace	14.18	Trace			91.89[c]
10	60.20	18.61	Trace		Trace	11.54	Trace			90.35[c]
11	53.72	22.96	0.50		0.31	13.46	0.1			91.05[c]
12	55.04	22.80	0.33		Trace	12.92	Trace			91.09[c]
13	53.06	24.27	0.58		0.77	12.5	0.97			92.15[c]

[a] Where only FeO values are given, they indicate total FeO + Fe_2O_3 contents

[b] The remainder consists of water (slightly above 8 wt%) and minor amout of Rb_2O, SrO and MnO (<1 wt%)

[c] 100 minus total denotes content of H_2O.

1–2 Analcite phenocrysts from feldspathoidal rocks occurring at northeastern Azerbaijan (Comin-Chiaramonti et al. 1997)

3–4 Analcites from Smoky Butte lamproites, Montana (Mitchell et al. 1987)

5–7 Analcites from leucite and analcite-bearing minette from Collima, Mexico. Analysis 6 is from Luhr and Carmichael (1981), who also reported presence of 0.01 wt% BaO. Other analyses are from Karlsson and Calyton (1991)

8 Analcite from potassic mafic lavas of the Bearpaw Mountains (Macdonald et al. 1992)

9–10 Analcite from Portobello (Wilkinson and Hensen 1994)

11–12 Analcite from Nombi (Wilkinson and Hensen 1994)

13 Analcite from Spring Mount (Wilkinson and Hensen 1994)

$NaAlSi_2O_6$). Wilkinson and Hensel observed that groundmass analcites in the basanites, mugearite and tinguaites from New Zealand, have relatively constant composition, approaching stoichiometric $NaAlSi_2O_6$. They also noticed the presence of an unusually Si-rich deutic analcite (60.2 wt% SiO_2) in vugs of the New Zealand tinguaites.

Wilkinson and Hensel (1994, Table 2.9, Fig. 2.13b) determined compositions of nephelines and analcites from different localities of the Bearpaw Mountains. These nephelines and analcites are from theralites [ST28 and ST20 (Fig. 2.13a)] and analcite tinguaites [ST40, ST16 and ST12 (Fig. 2.13b)] from Square Top, Portobello, Nombi and Spring Mount (Fig. 2.13c) (all from New Zealand). Their compositions are plotted as mole proportions with reference to $NaAlSiO_4$ (Ne)–$KAlSiO_4$(Ks)–SiO_2 (Qz) in Fig. 2.13. In this figure, dashed line (Barth line) denotes the Dollase-Thomas (1978) compositional trend of natural nephelines. The solid line marks the maximum limit for solid solution of feldspar in nepheline at 1,068 °C and 1 atmospheric pressure. This is extrapolated from the limit in the binary Ne–Qz system (Greig and Barth 1938). The dashed-dot line marks the limit of solid solution at 700 °C, 0.1 GPa P(H_2O) (Hamilton 1961). In the Fig. 2.13, nephelines (a and b) are denoted by circles and analcites by triangles (solid symbols refer to analyses made by Wilkinson and Hensel 1994). Analyses C–R (a) denote core and rim compositions of zoned nephelines in theralites ST28 and ST20, respectively. The point (Fig. 2.13c, circles) refer to nephelines (denoted by solid circles refer to analyses in Table 2.9, Nos. 1, 2), whereas solid triangle is groundmass analcite (Table 2.9, No. 5) in the Potobello analcite tinguaite. Points C and R denote the core and rim compositions of a zoned nepheline phenocrysts. The Portobello Si-rich analcite (Table 2.9, No. 6) falls outside the plot. Solid squares denote Nombi nephelines (Table 2.9, Nos. 5 and 6) and open squares refer to Nombi analcites (Table 2.9, Nos. 7, 8) linked by the tie-lines 3–5 and 4–6. The Spring Mount analcite (Table 2.9, No. 9) is represented by the solid diamond symbol.

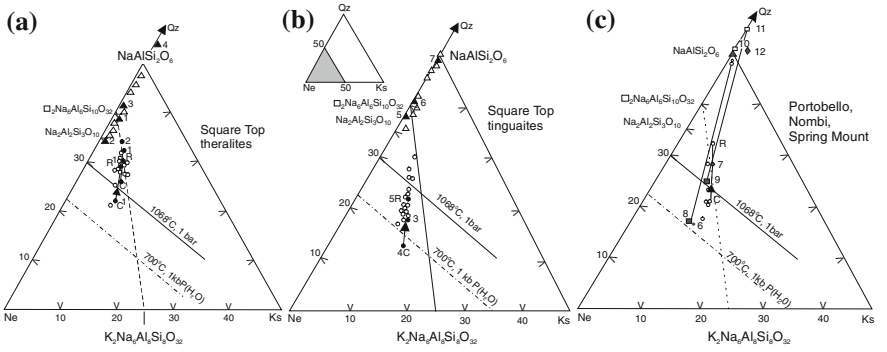

Fig. 2.13 Composition of nephelines and analcites from (**a**) Square Top theralites (ST28 and ST20), (**b**) analcite tinguaites (ST40, ST16 and ST12) and (**c**) Portobello, Nombi and Spring Mount hosts plotted as mole proportions of the components $NaAlSiO_4$ (Ne)–$KalSiO_4$ (Ks)–SiO_2 (Qz) (After Wilkinson and Hensel 1994)

Wilkinson and Hensel concluded that analcite and silica-undersaturated melt in the $NaAlSiO_4$–$KAlSiO_4$–SiO_2–H_2O system, cannot co-exist in equilibrium. Inferred solidus temperatures of the various hosts preclude a primary magmatic origin for the interstitial and groundmass analcites. These are interpreted as subsolidus phases produced by interaction of nepheline with deuteric and/or hydrothermal fluid (see also Gupta and Fyfe 1975). Analyses of nephelines and their derivative analcites indicate that the latter might have been formed from both Si-rich and more Si-poor nephelines.

Megascopic crystals of analcites are found in the Brown Leucitic Tuffs (Luhr and Giannetti 1987), where they often replace primary leucite phenocrysts. More basic leucite-bearing tuffs (CaO > 5.6 wt%) contain a lot of small analcite crystals, which are 0.02 mm across, but attain a size of 0.25 mm across in some pumices. Analcitization of leucite is a common geological phenomenon (Gupta and Fyfe 1975).

Analcites are often found in Tertiary extrusive rocks of north eastern Azerbaijan (Iran). At Harbab Khandi analcite occurs as well-developed crystals often replacing leucite in tephritic rocks. They are stoichiometric with respect to SiO_2, but are silica-oversaturated with reference to alkali. Analcites from Teic Dam and Razi are SiO_2-undersaturated and occur in three forms: (1) euhedral to subhedral or subrounded analcite in the groundmass, (2) weg-shaped subrounded analcite interfaced with large plagioclase phenocrysts in the groundmass (Table 2.9). Potassic analcite is an important phase in jumillites, fortunites and varites from southern Spain.

The presence of euhedral analcite has been described from dykes and lava flows of alkaline rocks at Pyatistennyl by Bazarova et al. (1981). Abundant micro-intrusives occur in this region, comprising leucite, analcite and pyroxene in a glassy matrix. Here, leucite and analcite coexist in the groundmass. The tuffs consist of leucite, orthoclase, plagioclase and augite.

Recently Jamtveit et al. (2009) studied replacement of leucite by analcite. They noted that a 10 % increase in volume is associated with the replacement process, and this generates stresses that eventually cause fracturing of the reacting leucite. Experimentally reacted leucite samples display characteristic fracturing patterns that include both spalling of concentric “onion-skin”-like layers near the reacting interface and the formation of cross-cutting, often hierarchically arranged, sets of fractures that divide the remaining leucite into progressively smaller domains. These structures may explain the “patchy” alteration patterns observed in natural leucite samples.

2.11 Melilite

Melilite compositions (Table 2.10) plot near the akermanite-sodamelilite join of the system akermanite-gehlenite-sodamelilite (Schairer and Yoder 1964; Schairer et al. 1965, 1967; Ferguson and Buddington 1920; Ferguson and Merwin 1919; Yoder 1973). Melilites containing small amount of $Ca_2FeSi_2O_7$ have been described from Capo di Bove Italy by Sahama (1974). He found that in the leucite-melilite

Table 2.10 Analyses of melilite from different ultrapotassic volcanic complexes (after Melluso et al. 1996)

	SiO_2	TiO_2	Al_2O_3	Fe_2O_3	FeO[a]	MgO	MnO	CaO	Na_2O	K_2O	SrO	H_2O+	Total
1	44.41	0.02	5.26		6.74	5.88	0.17	32.16	4.17	0.09			98.90
2	40.03		5.66	7.76	0.40	9.43		32.17	2.83	1.72			100.00
3	42.24	0.17	6.88	0.96	3.78	7.87	0.11	34.19	3.04	0.44			99.68
4	41.68		9.86	2.61	4.32	4.72		29.85	5.27	0.78		0.98	100.07
5	40.36		12.04	0.75	1.53	6.56		34.56	3.34	0.30		0.79	100.36
6	40.80	0.05	10.69		4.04	5.64	0.18	33.85	3.57	0.19	0.62		99.63
7	41.33		10.46		4.17	5.93	0.13	34.90	3.28	0.14	0.60		100.94
8	42.72	0.02	5.55		4.62	8.02	0.14	36.22	2.64	0.25	0.51		100.69
9	43.01		6.55		4.64	7.65	0.09	34.98	2.92	0.26	0.53		100.63
10	43.05	0.03	6.91		5.10	6.96	0.19	33.93	3.61	0.15	1.06		100.99
11	43.28		7.09		9.09	3.29	0.37	26.71	5.87	0.09	2.95		98.74
12	43.89		7.61		9.20	3.04	0.47	26.91	6.90	0.24	2.66		100.92
13	43.29	0.02	8.37		9.59	2.07	0.52	25.60	7.41	0.14	1.18		98.19

(continued)

Table 2.10 (continued)

	NaMel	Gehlen	Ak	NaFe									
6	32.80	12.50	54.70										
7	29.90	13.20	56.90										
8	24.80	2.50	72.70										
9	27.00	3.90	69.10										
10	32.00	2.10	65.90										
11	39.50		45.70	14.80									
12	41.50		36.60	21.80									
13	46.10		32.10	21.90									

[a] Where only FeO values are given, they indicate total FeO + Fe_2O_3 contents

1 Leucite-melilite-nephelinite volcano, Zaire (Sahama 1974)

2 Melilite from a K-rich olivine melilitite occurring at Capo de Bove, Italy (Buddington 1922)

3 Melilite from a K-rich rocks of Nyiragongo (Sahama and Meyer 1958)

4 Melilite from a K-rich melilite nephlinite lava from Roman province (Washington 1927)

5 Melilite from K-rich rocks of Monte Soma (Buddington 1922). Also contains 0.13 wt% H_2O

6–13 Melilites from Mt. Vulture volcanics (Melluso et al. 1996)

nephelinite lavas from Nyiragongo (Zaire), where it occurs as tiny crystal. These lavas also contain melilites, with prismatic habit, nearly perpendicular to the cavity wall. Stout prismatic melilite grains (up to 1 mm in length, averaging a few tens of a millimetre) occur in this region.

Melilite and leucite-bearing volcanic rocks occur at Mt. Vulture (Lucania, Italy). The place is located in the easternmost volcanic area of the Roman province. The most important melilite-bearing localities of this area include Prete Della Scimmia, whereas melilitite dyke is reported, and the other being Melfi hauynophyre lava flow. The flow occurs slightly outside a volcanic cone (Melluso et al. 1996).

The Prete Della Scimmia melilites are characterised by large, clear euhedral phenocrysts grading to microlites in the groundmass. In S. Caterina, melilite-melafoidites have melilites, occurring as a late groundmass phase, inter-grown with clinopyroxene, magnetite, leucite, nepheline and haüyne. At Melfi, melilite is present in haüynophyre as a light yellow-coloured groundmass phase with birefringence up to first order red and is optically negative.

The three melilite groups plot well within the field of volcanic melilites of Velde and Yoder (1977). The Pete della Scimmia melilites are very Mg-rich (up to 8 wt% MgO), alkali- and Al-poor melilites of the data set trend to become alkali-oversaturated with respect to Al (Fig. 2.14). Analysis shows that groundmass melilites contain 0.65 wt% (Ca, Na)$Fe^{3+}Si_2O_7$ (Na-ferrimelilite) having SrO contents as high as (0.5–1.5 wt%). In contrast, melilites from S. Caterina melilite-melafoidite lava flow, are gehlenite-rich (up to 13 mol%). The SrO contents are similar but slightly higher than melilites of Pete della Scimmia.

Of all the melilites those from Melfi haüynophyre are the most Na–Fe–Sr-rich ones found in Italy. Na-ferrimelilite molecule of these melilites can be as high as 22 mol % and the $CaNaAlSi_2O_7$ content is up to 46 mol%; the SrO content is high and they range from 3 to 1.18 %.

In sodium-rich leucite-bearing ultramafic rocks melilites were possibly formed by reaction between nepheline and diopside. It is observed that at 1.7 ± 0.3 GPa, melilite occurring as a reaction product of diopside and nepheline is eliminated (Singh et al. 2000). Akermanitic melilite breaks down even at atmospheric pressure and 690 °C to wollastonite and diopside (Yoder 1973), whereas at slightly higher

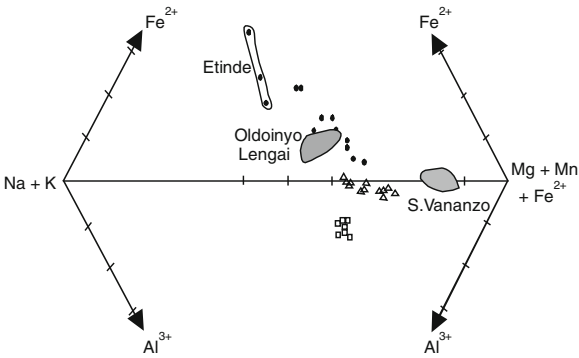

Fig. 2.14 Compositional plot of melilite in a (Na + K)–(Mg + Mn)–(Fe^{2+})–Al diagram (after Melluso et al. 1996)

pressures between 0.6 and 0.7 GPa, it breaks down to wollastonite and merwinite. Akermanite and gehlinite have a continuous solid solution relationship (Ferguson and Buddington 1920; Osborn and Schairer 1941). Sodamelilite is stable only above 0.4 GPa (Kushiro 1964), and at lower pressure it breaks down to nepheline and wollastonite.

Stopa et al. (2002) described the occurence of melilite-carbonetite rocks from the Apennines of Italy, where the rocks have paragenetic relationship with kamafugites of Grotto del Cervo, Abruzzo.

New discovery of leucite melilitites occurring as small lava flows and of kalsilite-melilite pyroclastic ejecta has been described from Montefiascone Volcanics complex of Roman Magatic Province of Central Italy by Di Battistini et al. (2001).

2.12 Haüyne

The chemical composition of Haüyne lies between nosean ($Na_8Al_6Si_6O_{24}SO_4$) and a hypothetical end member ($Ca_4Al_6Si_6O_{24}.SO_4$). It has a cubic symmetry. Some haüynes have minor replacements of Al by Fe^{3+} but the substitution of K for Na is more important in haüyne.

This mineral occurs in potassic lavas of the Roman province, central Italy (Table 2.11). At Melfi, haüynes have a relatively high content of K_2O. Haüyne often displays chemical zoning and its alumina content increases towards the core (De Fino et al. 1986). It has also been reported from phonolitic rocks at Sabatini by Cundari (1979). It occurs as "murky" phenocrysts with characteristic reddish rims.

In the Mt. Vulture volcanic rocks haüyne is a very common feldspathoid, where it occurs together with smaller amounts of leucite. Nepheline is present only as a groundmass phase in melilite-bearing rocks, and is very rare in the feldspar-bearing rocks.

Black oriented inclusions are often noted in haüyne, where it is often concentrated towards the rims. It often has a thin film at the outer rim which is inclusion-free, and has large core-to-rim and "inter-sample" variations. The SO_3 concentration varies from 11.6 to 6.78 wt%, with a clear decrease of SO_3 content from the core to the rim. Melluso et al. (1996) suggested frequent substitution of SO_3 by Cl, which is coupled with Na-enrichment. This gives evidence for increasing sodalite contents. K and Ca do not show clear trends, even though the most Ca–K, and Sr-rich haüynes are found in relatively poorly differentiated samples (basanites and tephrites). The haüynes of the phonolites are characterised by low Ca, K and SO_3 contents, decreasing towards the rims and/or to the groundmass. In melilite-bearing rocks however, the haüynes have sulphur. Caterina melilite-mela-foidite show relatively high Ca and K contents coupled with low SO_3 (7 wt%). The Melfi haüynophyre shows a higher variation in K_2O (SO_3 content varying from 6.60 to 1.8 wt%) but without coherent trends from core to the rim (De Fino et al. 1986).

Di Muro et al. (2004) studied hauynophyre bearing lava from Mount Vulture Italy. They collected a sample from a parasitic vent of the Vulture stratovolcano.

Table 2.11 Analyses of Haüyne from Monte vulture and roman province of Italy

	SiO_2	Al_2O_3	Fe_2O_3	FeO	CaO	SrO	Na_2O	K_2O	SO_3	Cl	H_2O	Total
1	33.62	28.52	0.70	0.76	5.43		17.07	3.80	9.39	0.29	1.65	101.23
2	33.50	27.40	0.32		7.90	0.22	16.30	1.20	12.50	0.46		99.80
3	33.20	26.90	0.40		7.20	0.15	14.60	5.10	11.40	0.62		99.57
4	33.10	26.50	0.34		6.50		14.50	5.90	12.00	0.52		99.36
5	39.20	31.20	0.28		0.24		23.00	1.30	6.40			101.62
6	38.00	29.80				0.10	22.80	1.10	6.90			98.70

1 Haüyne from Monte Vulture (Francalanci et al. 1987)
2–4 Haüyne from Roman Province (Balridge et al. 1981)
5–6 Sodalite from Roman Province (Balridge et al. 1981)

It is a S- and Cl-rich, leucite-melilite-bearing lava flow containing an unusually large amount of sodalite group of minerals (>23 vol%). Mineralogical and chemical study of phenocrysts has led to the identification of black haüynes, blue lazurites and of Cl-rich white or black noseans. X-ray diffraction (XRD) study confirms the occurrence of nosean having a low symmetry (P23). Raman spectra and XRD data show that S is fully oxidised to SO_4 in black haüynes and in white noseans, while it is partly reduced to form S_3^- groups in blue lazurites, which also contain H_2O molecules. Among euhedral phenocrysts, large lazurites are only faintly zoned. All other phases show variable core-rim chemical zoning and many phenocrysts are partially resorbed and/or colour-zoned. Black haüynes have highly variable S/Cl and slightly lower SiO_2/Al_2O_3 ratios, larger $Fe_{(TOT)}$ contents and more compatible trace elements than lazurites. Thin opaque nosean-sodalite rims surrounding all crystals are interpreted as a result of rapid crystallization driven by exsolution of a S-scavenging fluid phase.

2.13 Apatite

High REE content of potassic rocks is mainly due to the presence of apatite, which is a very common accessory mineral. Apatites from Leucite Hills, Wyomintg (U.S.A., Kuehner et al. 1981) contain 0.12–0.27 % La_2O_3, 0.41–0.65 % Ce_2O_3, 0.07–0.9 % Pr_2O_3 and 0.24–0.41 % Nd_2O_3 (all in wt%) (Table 2.12). Over 3 wt% of Ca in some of the apatites is replaced by the Ce-group of rare earth elements. There is often replacement of Mn, Sr and rare earth elements for Ca (Table 2.12). Apatites from the lamproitic rocks of West Kimberly, Australia are also characterised by high REE contents.

In minettes from Highwood Mountains micro-phenocrystal apatites occurs commonly (O'Brien et al. 1991). It ranges in composition from chloro-hydroxy-apatite to fluor-apatite. Rare earth element content of this phase is typically high (0.4 and 0.6 wt% La_2O_3 and Ce_2O_3, respectively). Variable F, Cl and (OH) contents in apatites imply a complex degassing history of Highwood Mountains magmatic system.

In the groundmass glass of Brown Leucitic Tuff of Roccamonfina, Italy (Lhur and Giannetti 1987), apatite (up to 0.55 mm across) is a common mineral. The F, Cl and H_2O contents of these apatites are 2.41, 0.16 and 0.58 wt%, respectively. It is enriched in SrO (Table 2.12).

2.14 Spinel

Jaques and Folley (1985) observed that aluminous spinels (pleonaste-hercynite) occur as inclusions (mostly <20 μm but rarely >40 μm) in leucite phenocrysts of the Fitzory area, Western Australia. These inclusions could be readily recognised in

Table 2.12 Analyses of apatite

	SiO_2	TiO_2	FeO_t[a]	MnO	MgO	CaO	SrO	BaO	Na_2O	K_2O	P_2O_5	Cl	F	−F = 0	Total
1		0.33	0.30		0.40	54.63			0.03	0.21	36.91	0.02	5.01		98.04
2			0.42	0.03	0.27	55.10	0.22	0.04	0.10	0.62	41.70	0.04	2.78	1.17	100.15
3			0.48	0.05	0.14	54.30	0.59	0.06	0.15	0.59	41.20	0.09	3.11	1.31	99.45
4	0.99		0.19	0.03	0.10	54.98	0.58		0.23		40.37	0.16	2.41		99.60
5	0.05	0.69	0.33	–	0.00	48.05	2.07	12.20	0.15	0.11	36.50	–	0.00	–	100.01
6	0.49	–	0.30	0.03	0.31	54.10	0.29		0.15		40.10	0.75	3.30		100.40
7	0.60		0.46	0.02	0.32	53.90	0.28		0.16		40.00	0.76	1.40		100.50

[a] FeO_t indicates total FeO + Fe_2O_3 contents

1 Apatite from a lamproitic rock at Mohanpur, Damodar valley, India (Gupta et al. 1983). Also contains 0.2 wt% Al_2O_3

2–3 Apatite from an ultrapotassic basanitic lava, Sierra Nevada, U.S.A. (van Kooten 1980)

4 Apatite from a leucitic tuff, Roccamonfina, Italy (Luhr and Giannetti 1987). Also contains 0.03 wt% Al_2O_3 and 0.58 wt% H_2O

5 Barian fluorapatite, diopside-leucite lamproite, West Kimberley, Western Australia (Edgar 1989)

6 Apatite from K-rich rocks of Vesuvius, lava of1760 eruption, Ungino, Italy (Baldridge et al. 1981). Also contains 0.03 wt% SO_3, 0.12 wt% La_2O_3, 0.22 wt% Ce_2O_3, 0.14 wt% Nd_2O_3 and 0.06 wt% Al_2O_3

7 Apatite from K-rich rocks of Vesuvius, 1631 lava, La Scala, Italy (Baldridge et al. 1981). Also contains 0.11 wt% SO_3, 0.10 wt% La_2O_3, 0.20 wt% Ce_2O_3, 0.15 wt% Nd_2O_3 and 0.08 wt% Al_2O_3

fresh leucites, but could also be observed in lamproites, where the leucite is replaced and pseudomorphed by K-feldspar, zeolites etc. The alumina spinels (Table 2.13) occur as amoeboid-shaped to strongly rounded larger crystals. The spinel inclusions are found to be low in Cr content (<0.2 %, commonly <0.1 % Cr_2O_3). According to Jaques and Foley (1985) these spinels have highly contrasting compositions with high Cr content in the titanium magnesio-chromites occurring in the groundmass (Fig. 2.15).

Pleonaste, the Fe-rich variety of spinel, was found in the wyomingites from Leucite Hills (Table 2.13) by Kuehner et al. (1981). They also described the presence of magnesio-chromite (Table 2.13) having high Fe_2O_3/FeO ratio and low TiO_2 content.

Jaques and Foley (1985) have reported the occurrences of titano-magnetites (Table 2.13) as euhedral or skeletal crystals in all K-rich volcanic rocks of Western Australia, where it is found either as a late stage oxidation product of olivine, mica, K-richterite or clinopyroxenes. Ti-rich magnesio-chromite has also been described from the lamproitic rocks of Fitzroy basin, Western Australia (Jaques and Foley 1985).

Perovskite from minettes of Highwood Mountains (O'Brien et al. contains 12.8 % TiO_2 (Table 2.13), which is equivalent to 36.7 mol% of ulvospinel.

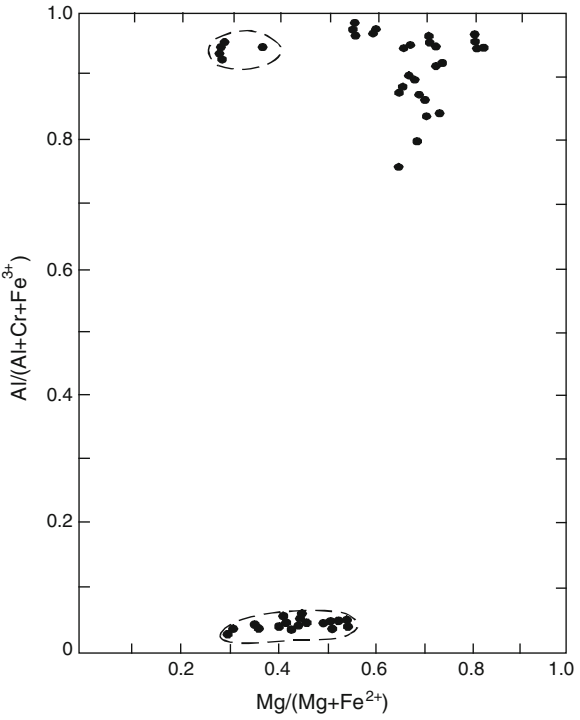

Fig. 2.15 Compositions of aluminous spinel inclusions in leucite in West Kimberley leucite lamproites contrasted with groundmass titanian magnesio-chromites in terms of $Al/(Al + Cr + Fe^{3+})$ versus $Mg/(Mg + Fe^{2+})$ (after Jaques and Foley 1985)

Table 2.13 Analyses of Spinel occurring in Different K-rich rocks from different localities

	SiO_2	FeO_t	TiO_2	Al_2O_3	Cr_2O_3	P_2O_5	MgO	MnO	CaO	Na_2O	K_2O	ZrO_2	ZnO	Total	Fe_2O_3	FeO[a]
1	0.02		0.05		0.02							0.03	0.06	78.41		78.23
2	0.09		18.95	3.36	0.11		2.27	0.44	0.29					93.48		67.97
3			1.77	2.80			1.61	0.51	0.03					91.73		85.01
4	0.36		15.03	3.19	0.15		2.01	0.99		0.18				89.51		67.60
5			12.00	0.27	0.57	0.91	1.95	0.54	0.04	0.10	0.30		0.42	95.40		78.30
6			7.02	0.68	1.00	0.56	4.44	0.59	0.10	0.04	0.24		0.21	94.58		79.70
7			13.00	5.21	0.55	0.91	2.83	0.88	0.05	0.06	0.19		0.28	95.96		72.00
8	0.12		0.21	64.87	0.23		21.77	0.05	0.02					100.50		13.23
9	0.05		0.24	63.60	0.16		14.59	0.09	0.02					100.61		21.86
10	0.10		6.79	3.56			0.67	1.49		0.02				99.33	51.36	35.34
11	0.03		5.22	4.12	0.01	0.45	2.07	0.65						93.70		81.15
12	n.d.		6.55	3.03	0.01	0.51	1.85	0.77						95.02		82.30
13	n.d.		4.28	1.96	n.d.	0.44	0.41	0.60						94.08		86.39
14			0.11	11.93	57.52		15.33	0.93						99.59		13.77
15			0.68	6.71	44.07		10.79	0.79						95.85		32.81
16			0.02	64.53	0.10		20.32	0.06						99.35		14.32
17	0.03		0.38	57.66	0.02		7.46	0.16						99.73		34.02
18	0.05		4.33	2.16	55.20		7.15	0.93						99.50		29.68
19		37.05	4.52	0.23	51.41		4.42	0.84						98.47	9.77	28.26
20		20.33	1.23	3.04	65.34		10.41	0.69						101.04	3.22	17.43

(continued)

Table 2.13 (continued)

	SiO_2	FeO_t	TiO_2	Al_2O_3	Cr_2O_3	P_2O_5	MgO	MnO	CaO	Na_2O	K_2O	ZrO_2	ZnO	Total	Fe_2O_3	FeO[a]
21		29.34	1.03	2.00	55.78		9.80	0.79						98.74	13.32	17.35
22		15.31	2.14	4.16	63.00		13.80	0.48					0.2	99.09	2.97	12.64
23		47.95	5.70	1.87	36.22		3.30	0.86						95.90	19.27	30.61

[a] Where only a few values are given, they indicate total FeO + Fe_2O_3 contents

1 Magnetite from a nepheline and leucite-bearing tephrite, Laacher See, Germany (Duda and Schminke 1978)
2 Magnetite from a leucite basanite, Laacher See, Germany (Duda and Schminke 1978)
3 Magnetite from a leucite tephrite, Laacher See (Duda and Schminke 1978)
4 Magnetite from a phonotephrite, Alban Hills, Italy (Aurisicchio et al. 1988)
5–7 Magnetite from lamproites of Sierra Nevada (van Kooten 1980)
8–9 Pleonastes from a leucite lamproite (Fitzroy, Western Australia), Jaques and Foley 1985)
10 Titanomagnetite from a leucite phonololite from Vulsini lava, Italy (Francalanci et al. 1987)
11–13 Titanomagnetites from a Leucitic tuff, Roccamonfina, Italy (Luhr and Giannetti 1987)
14–15 Magnesiochromites from an olivine orendite, South Table Mountain Leucite Hills (Kuehner et al. 1981)
16 Pleonaste from a wyomingite, Deer Butte, Leucite Hills (Kuehner et al. 1981)
17 Hercynite, aggregate in a leucite lamproites from Fitzroy, Western Australia (Jaques and Foley 1985)
18 Titanferous magnesiochromite from a lamproite, Fitzroy, Western Australia (Jaques and Foley 1985)
19–21 Representative microprobe analyses of chrome spinel from a Cancsrix lamproite, Albacete Spain (Wagner and Velde 1986)
22 Representative microprobe analyses of chromian spinel from a Sisco lamproite, Corsica. (Wagner and Velde 1986)
23 Representative microprobe analyses of chrome spinel from an Orciatico lamproite, Pisam, Italy (Wagner and Velde 1986)

Authigenic olivines often contain chromites as inclusions (Table 2.13). They are characterised by higher Cr_2O_3, lower Al_2O_3 and higher Mg/(Mg +Fe) ratio, compared to chromites found by Danchin and Boyd (1976) in harzburgites. Their low Al content is related to the peralkaline chemistry of the magma. Their high Cr content could be related to the low Al and Fe^{3+} contents of the liquid. Chromites are described from the lamproitic rocks of Cancarix (Albacete); Calasparra (Murcia), Jumilla (Murcia), Barqueros (Murcia), Smoky Butte (Montana, U.S.A.), Sisco (Corsica) and Orciatico (Italy) (Table 2.13), often contain titano-magentites ranging in composition from 16 to 0 wt% Cr_2O_3, 7 to 0.7 wt% MgO, 7 to 4 wt% Al_2O_3, and 2 to 5.4 wt% TiO_2.

In the Brown Leucite Tuffs of Roccamonfina, euhedral Ti-magnetite phenocrysts (up to 0.6 mm across) occur. In these rocks it is found as inclusions in salites. The MgO (0.41–2.70 wt%), Cr_2O_3 (trace to 0.01 wt%) and Al_2O_3 (1.96–4.25 wt%) content of titano-magnetites are variable.

Cundari (1975) observed that the Fe–Ti oxides from Vico lavas are ubiquitous, as accessory minerals. They occur as equant-shaped phenocrysts as well as microlites or micro-phenocrysts (Cundari 1975) in the groundmass. They noted that the TiO_2 content increases from 5.2 to 13.1 wt% and MnO up to 2.5 wt%. Melluso et al. further noted that the increase of ulvospinel and magnetite components are inversely proportional to Mg and Al contents, but are positively correlated with respect to Mn. In lamproitic rocks chromian spinels are present as a late stage product in the lamproitic rocks of Damodar Valley (India). It is found in most of the dykes of Raniganj, Jharia and Bokaro coal field. Spinel is a ubiquitous phase in the Mt. Vulture volcanic complex, where it occurs as small microphenocrysts, poikilitically enclosed by clinopyroxenes, or it may occur as a small cubic crystals included within olivines. Melluso et al. (1996) observed that these latter spinels are heterogeneous within the same olivine grains and range from Cr-rich (36 wt% Cr_2O_3) to Cr-free variety. The spinels found in the groundmass or included in clinopyroxenes contain variable amounts of Al_2O_3 (13–0.8 wt%) with highest values observed in basanites, but decreasing towards phonolites. They noted that the TiO_2 content increases from 5.2 to 13.1 wt% and MnO up to 2.5 wt%. Melluso et al. further noted that the increase of ulvospinel and magnetite components are inversely proportional to Mg and Al contents, but are positively correlated with respect to Mn. In lamproitic rocks chromian spinels are present as a late stage product in the lamproitic rocks of Damodar Valley (India). It is found in most of the dykes of Raniganj, Jharia and Bokaro coal field.

2.15 Priderite

This mineral typically occurs as an accessory phase in lamproitic rocks. Priderite has tetragonal symmetry with a structure similar to that of a cryptomelane (KMn_8O_{16}) with a general formula of ($A_{2-x}B_{8-y}O_{16}$). *X* stands for K and Ba, and *Y* represents such elements as B, Ti, Fe and Al (Carmichael 1967). He observed that

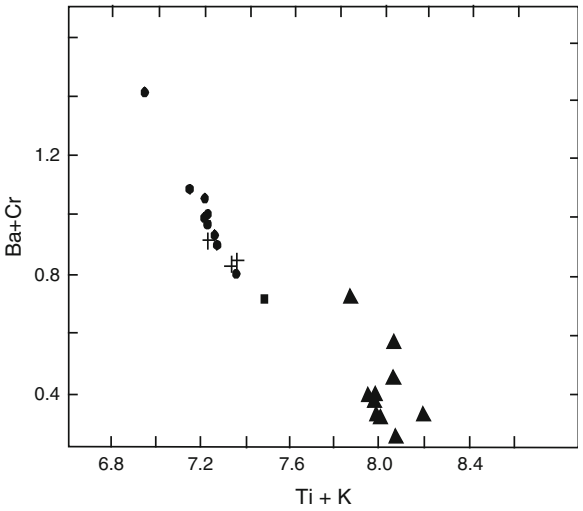

Fig. 2.16 The distribution of Ba + Cr and Ti + K in priderites. *Solid circles*: Smoky Butte lamproite, Montana; *plus symbol*, priderite from Sisco minette, Corsica, (France); *solid triangles*: priderite from wolgidite, Mount North, West Kimberley; *solid squires*: Leucite Hillis lamproite (after Wagner and velde 1986)

priderite from Leucite Hills contains more Ba than that from West Kimberley. They may have a solid solution relationship between K-priderite and Ba-priderite (Norrish 1951). Priderite in association with ilmenite is observed in Mt. North lamproite from Australia and Sisco Minette from Corsica (Wagner and Velde 1986). Analyses of priderites show that (Ba + Cr) has a negative correlation with respect to (Ti + K, Fig. 2.16).

Smoky Buttte lamproites often contain priderites (Post et al. 1982). It is enriched in Ba (up to 0.85), but K is only 0.4 per formula unit. It contains 4.3 wt% Cr_2O_3 in West Kimberley and Smoky Butte lamproites, respectively, but it can be Cr-poor also (<0.3 wt%, Table 2.14). The high Ba values suggest the existence of Ba end member of the priderite series.

This mineral has also been described as an accessory phase from lamproitic rocks of Mohanpur (West Bengal, India; Gupta et al. 1983), and Kapamba, Luangwa valley (eastern Zambia, Scott Smith et al. 1987).

2.16 Wadeite

Prider (1939) described wadeite for the first time from K-rich rocks of West Kimberley province. Henshaw (1955) determined its crystal structure, and found that it has hexagonal symmetry and high birefringence. Its ideal formula is $Zr_2K_4Si_6O_{18}$. The structure is constituted of rings of $(Si_2O_9)^{6-}$, similar to benitoite. It is also present (Table 2.15) as an accessory mineral in the ultrapotassic rocks of Leucite Hills (Carmichael 1967).

Table 2.14 Analyses of priderite

	SiO_2	TiO_2	Al_2O_3	Fe_2O_3	FeO[a]	MgO	CaO	MnO	BaO	Na_2O	K_2O	Cr_2O_3	Total
1	0.00	79.27	0.10		8.94	0.13	0.19	0.04	1.10	0.14	8.10	0.22	98.32
2	–	73.30	0.03		11.40	0.90	0.04	0.06	5.80	0.02	7.40		99.5
3	–	70.60	2.30		12.40	–	0.6	–	6.70	0.06	5.60		98.2
4	–	67.80	0.04		12.60	0.80	0.07	0.40	13.10	0.07	5.0		99.2
5	n.d.	81.56	0.02		9.51				0.26		8.65	0.42	100.42
6	n.d.	78.86	0.05		9.62				0.76		9.59	0.48	99.36
7		78.89		9.19		0.74			6.30		7.15	4.36	100.63
8		68.18		9.09		1.02			16.73		2.73	1.85	99.60
9		71.46		10.75		0.17			16.39		2.27		101.04

[a] Where only a few values are given, they indicate total FeO + Fe_2O_3 contents

1 Priderite from a Damoder valley lamproite (Gupta et al. 1983). Also includes 0.09 wt% NiO

2 Priderite from a West Kimberley lamproite (Wade and Prider 1940)

3 Priderite from a West Kimerley lamproite (Norrish 1951)

4 Priderite from a Leucite Hills lamproite (Carmicheal 1967)

5–6 Two pridirites from a Holsteinborg lamproite, West Greenland (Scott Smith, B.H. 1981)

7 Priderite from a lamproite occurring at Mount North, West Kimberley, Australia (Wagner and Velde 1986)

8 Priderite from a lamproite occurring at Smoky-Butte, Montana, U.S.A. (Wagner and Velde 1986)

9 Priderite from a lamproite at Sisco, Corsica, France (Wagner and Velde 1986)

Table 2.15 Analyses of wadeite from K-rich rocks

	SiO_2	TiO_2	ZrO_2	Al_2O_3	Fe_2O_3	FeO	MgO	CaO	SrO	Na_2O	K_2O	BaO	P_2O_5	H_2O	Total
1	48.80	2.80	27.90	0.20		0.40		0.10		0.10	19.70	0.10			100.10
2	47.40	0.80	28.50	0.80	Trace	0.60		0.10		0.10	21.50	0.10			99.90
3	39.43	1.63	21.29	5.98			0.28	5.22	0.16	2.82	18.40	1.20	3.15	1.30	100.86

1–2 Wedeites from lamproitic rocks, West Kimberly, Australia (Wade and Prider 1940)
3 Wadiate from a lamproitic rock occurring Leucite Hills (Carmichael 1967)

It is stable under following P–T conditions: 1.2 GPa (800, 1,000 °C), 1.4 GPa (1,000 °C), 1.5 GPa (1,000–1,200 °C), 1.75–1.88 GPa, (1,200 °C), 2.0–2.2 GPa (1,200 °C) and 2.5 GPa (1,200 and 1,250 °C) (Arima and Edgar 1980).

2.17 Roedderite-Like Mineral [$(Na, K)_2(Mg, Fe)_5Si_{12}O_{30}$)]

Roedderite-like minerals have been described from the lamproitic rocks of Cancarix, Albacete (Spain) and Moon Canyon, Utah (U.S.A.). This is a blue mineral (Table 2.16), belonging to roedderite-eifelite series (Abraham et al. 1983). The mineral from Cancarix is a sodium-free but iron-rich phase relative to those found in Eifel, Germany. This is a rare mineral, which is crystallised from the melt. The same phase is quite abundant in the Moon Canyon lamproite (Wagner and Velde 1986), but is less iron-rich but more enriched in Mg and Na than that from Cancarix.

Wagner and Valde (1986) suggested a substitution of the type, $Fe^{3+} \rightleftharpoons Fe^{2+} + Na^{+}$ but entry of Fe^{3+} in the structure creates a vacant site (an alkali site). Wagner and Valde suggested that the deep blue colour in the mineral may be due to the presence of Fe^{3+}. A similar phase (eifelite, Abraham et al. 1983) has been described from the K-rich volcanic ejecta of Eifel, of Germany.

2.18 Pseudo-Brookite

This mineral is a solid solution of the end members Fe_2TiO_5 (Pseudo-brookite), $FeTi_2O_5$ (ferro-pseudo-brookite), $MgTi_2O_5$ (karooite) and Al_2TiO_5. Pseudobrookite is present as an euhedral plate, hexagonal in shape. They are green or purple brown, usually opaque, but sometimes translucent (e.g. Smoky Butte lamproite, Wagner and Velde 1986). They exhibit reddish internal reflection under reflected light.

Table 2.16 Analyses of roedderite-like mineral

	SiO_2	Al_2O_3	FeO[a]	MgO	MnO	TiO2	Na_2O	K_2O	Total
1	70.29		12.60	11.44	0.23	0.02	0.04	4.48	99.10
2	69.86	0.17	9.83	13.90	0.21	0.21	0.25	5.14	99.57
3	70.60	0.50	5.80	15.70	0.21	0.07	1.80	4.20	98.88
4	71.32	0.36	0.49	17.86	0.31	0.07	5.29	4.16	99.86

[a] FeO indicates total FeO + Fe_2O_3

1 Representative electron microprobe analyses of the roedderite-like phase, from Cancarix lamproite, Albacete, Spain (Wagner and Velde 1986)

2 Representative electron microprobe analyses of the roedderite-like phase, from Moon Canyon lamproite, Utah, U.S.A. (Wagner and Velde 1986)

3–4 Roedderite in Volcanic ejecta, Eifel region Germany (Hentschel et al. 1980)

Table 2.17 Analyses of pseudobrookite from lamproites of different localities (after Wagner and Velde (1986)

	Al_2O_3	Cr_2O_3	FeO_t^a	MgO	MnO	TiO_2	Total	Fe_2O_3	FeO
1	0.02	0.82	28.97	8.65	0.33	60.33	99.12	26.38	5.24
2	0.47	0.43	19.66	9.39	0.15	69.02	99.12	8.57	11.94
3	0.30	0.99	19.86	8.92	0.14	69.04	99.25	7.71	12.92
4	0.06	0.05	23.46	7.61	0.20	66.12	97.50	11.03	13.54

[a] FeO_t indicates total FeO + Fe_2O_3 contents
1 Pseudobrookite from a Cancarix lamproites, Albacete Spain
2 Pseudobrookite from a Barqueros lamproite, Murcia, Spain
3 Pseudobrookite from a Smoky Butte lamproite, Montana, U.S.A.
4 Pseudobrookite from a Moon Canyon lamproite, Utah, U.S.A.

Around 40 % of this mineral is ferro-pseudobrookite (12–15 % pseudobrookite and 42–48 % karooite, Table 2.17). In some of the lamproites from Murcia (Spain), the pseudobrookite is very rich in MgO (up to 52 mol% karooite component), and it resembles armalcolite.

2.19 Perovskite

Wade and Prider (1940) reported the presence of perovskite as an accessory mineral in association with K-richterite in leucite-bearing rocks of West Kimberley. It is present as a small dark reddish brown mineral with high relief. The pervoskites from lamproitic rocks of Leucite Hills are enriched in Ce. Sr, Na and K. The presence of high concentration of La_2O_3 (2.03–2.05 wt%), Ce_2O_3 (4.45–4.87 wt%), Pr_2O_3 (1.47–1.64 wt%) and Nd_2O_3 (1.73–1.91 wt%) has been described by Kuehner et al. (1981, for major element chemistry, see Table 2.18).

In Prete della Scimmia, perovskite occurs as inclusions in green clinopyroxenes contained within melilitite rocks. The low totals of the microprobe analyses may be related to high REE contents. They show lower SrO (0.22–0.45 wt%) than that of the co-existing apatites (1.2 wt%).

2.20 Ilmenite

In lamproites, ilmenite occurs as a common mineral after olivine, clinopyroxene and phlogopite. They are poor in Fe_2O_3 and constitute about 64–90 vol% $FeTiO_3$ component, 11–30 % geikelite and 1–2 wt% pyrophannite. The lamproites from Barqueros (Murcia, Spain) contain Mg-ilmenite with a rutile core.

Table 2.18 Analyses of melanite and Mg-rich ankarite

	SiO_2	TiO_2	Al_2O_3	Fe_2O_3	FeO[a]	Re_2O_3	SrO	MnO	MgO	CaO	Na_2O	K_2O	CO_2	Total
1	35.70	2.64	10.30	17.10				1.31	0.19	32.80				100.04
2	32.50	5.72	5.81	22.30				0.86	0.31	32.50				100.00
3	32.82	7.19	4.84	19.44				0.85	0.21	32.18	0.08			97.61
4	27.03	17.49	1.59	19.39				0.52	1.13	31.67	0.02			98.84
5		0.03	0.02		5.45			0.02	17.07	26.44		0.01	49.24	98.32
6		48.70	0.03		7.70	11.40	5.70			23.50	2.50	0.60		100.13
7		48.20	0.05		11.40	10.60	3.80			25.10	1.00	0.30		100.45

[a] FeO indicates total FeO + Fe_2O_3 contents

1–2 Melanite garnets from a leucite-tephrites, Tavalato, Rome (Baldridge et al. 1981)

3–4 Melanite garnets from a melilitite lava occurring at Prete Della Scimmia, Mt. Vulture (Melluso et al. 1996)

5 Magnesium ankarite from a lamproite occurring at Mohanpur, Damodar Valley coal field (West Bengal, India, Gupta et al. (1983). Also contains 0.02 wt% Cl and 0.02 wt% P_2O_5

6–7 Perovskites from lamproitic rocks of Leucite-Hills, Wyoming (U.S.A.) (Carmichael 1967). Re_2O_3 refers to Rare Earth Oxides

2.21 Melanite

In leucite phonolites at Tavalato (Italy), melanite occurs both as a phenocryst as well as groundmass mineral. These phenocrysts are zoned with colourless cores having pale–yellowish–brown margins. The analyses show that they are poor in MgO, and that there is not only a significant increase in the TiO_2 and Fe_2O_3 contents but also there is a corresponding decrease in the Al_2O_3 content in the rims of the phenocrysts and groundmass phases. Melanite garnets (Table 2.18) have also been described from a melilitite lava flow at Mt. Vulture (Melluso et al. 1996).

2.22 Carbonate-Bearing Phases

Ankerite phenocysts in association with phlogopite occur in the lamproitic rocks from the Raniganj Basin, India (Table 2.18, analyses no. 5). The other accessory minerals include apatite and chromian spinal in a groundmass of the same phases along with rutile, pyrite and devitrified glass (Gupta et al. 1983). These lamproites are so much enriched in carbonates (10–15 vol%, ankarite), and phlogopite (55–60 vol%), that they termed these rocks as carbonated apatite-bearing glimmerites. Basu et al. (1997) studied the lamproitic rocks of Bokaro basin (Damodar Valley, India). They also noted the presence of $MgCO_3$-rich carbonate phases in these lamproites.

http://www.springer.com/978-81-322-2082-4

Origin of Potassium-rich Silica-deficient Igneous Rocks

Gupta, A.K.

2015, XXIII, 536 p. 229 illus., Hardcover
ISBN: 978-81-322-2082-4